sustainability

MDPI

Review

Novel Applications of Silk Proteins Based on Their Interactions with Metal Ions

Qingmei Wen [1,†], Lei Zhang [2,†], Yilu Chen [3], Yi Su [4], Jingmou Yu [2], Pu Chen [2,*] and Tao Zheng [1,*]

[1] Guangzhou Institute of Energy Conversion, Chinese Academy of Sciences, Guangzhou 510640, China; wenqm@ms.giec.ac.cn
[2] Department of Chemical Engineering and Waterloo Institute for Nanotechnology, University of Waterloo, Waterloo, ON N2L 3G1, Canada; l78zhang@uwaterloo.ca (L.Z.); j532yu@uwaterloo.ca (J.Y.)
[3] Jiangsu Ecogreen Biotechnology Institute, Nanjing 211100, China; helloyilu@foxmail.com
[4] Zhejiang Ecogreen Ecological Technology Co., Ltd., Huzhou 313000, China; suyi@ecogreen.tech
* Correspondence: p4chen@uwaterloo.ca (P.C.); zhengtao@ms.giec.ac.cn (T.Z.)
† These authors contributed equally to this work.

Abstract: Silk secreted by *Bombyx mori* L. silkworm has become one of the most important biomaterials, due to its excellent biocompatibility, controllable biodegradability, superior processability, and unique mechanical properties. Silk fibroin and sericin, as the two components of silk, contain abundant polar functional groups, and thus can bind metal ions through electrostatic interaction and chelation. Based on this binding, silk proteins not only can be used to fabricate ecofriendly and efficient adsorbents to remove heavy metals from waterbodies, but also can synthesize metal nanostructures (nanoparticles or nanoclusters) to form silk/metal composites with amazing optical or electrochemical characteristics. This binding also can be manipulated to optimize silk's performance. This review focuses on discussing and summarizing advances in the use of silk fibroin and sericin for heavy metal ion-contaminated water remediation, biosensing materials, and electrochemical materials from the perspective of the interaction between silk proteins and metal ions. The performance enhancement of silk using metal ions is also analyzed. Moreover, the silk proteins' interactions with metal ions and related structural features that contribute to the above sustainable applications are illustrated to lay a theoretical foundation. This review will favor the expansion of the applications of silk in both the traditional textile field and new biomaterials.

Keywords: silk protein; silk peptide; metal ion; mechanical property; heavy metal-contaminated water remediation; biosensing; electrochemical

Citation: Wen, Q.; Zhang, L.; Chen, Y.; Su, Y.; Yu, J.; Chen, P.; Zheng, T. Novel Applications of Silk Proteins Based on Their Interactions with Metal Ions. *Sustainability* **2023**, *15*, 16053. https://doi.org/10.3390/su152216053

Academic Editor: Asterios Bakolas

Received: 9 October 2023
Revised: 6 November 2023
Accepted: 13 November 2023
Published: 17 November 2023

1. Introduction

The silk spun by *Bombyx mori* L. silkworms has been used as a textile material in China for nearly four thousand years [1,2]. The pristine silk fiber is composed of a core of silk protein, silk fibroin (SF), and an outer layer of silk protein, silk sericin. The sericin wraps the SF. SF is obtained from a degumming process to remove the sericin and is the component used for textiles, while sericin is usually discarded as waste [3]. Today, the use of silk proteins has expanded from the textile field to many new fields, including environment remediation, bioengineering, and intelligent electronics, due to their outstanding mechanical properties, biocompatibility, biodegradability, and processibility [4,5].

The fabrics made with SF are lightweight, and feature air permeability and a charming luster [6]. Nevertheless, with the increase in silk fabrics' use in both the commodity textile world and high-tech fields, and the change in human aesthetic conceptions, silk is gradually unable to meet new needs in aspects of mechanical properties, color fastness, and flame retardancy, which promote researchers to modify the properties of silk [7]. Therefore, silk is used in combination with other functional materials, or its morphology or components are changed [8–11]. These investigations hope to enhance the mechanical properties, flame

retardancy, and color fastness of silk fabrics, and at the same time, maintain some intrinsic properties, like the appealing luster, to cater to new application scenarios.

Regarding the optimization of silk's mechanical properties, intrinsic and extrinsic technologies have been used by researchers [12,13]. The intrinsic method means modifying the genetic sequences of silkworms since silk's properties highly depend on the amino acid coding sequences and conformation [14,15]. Generally, genetic modification is complicated and very expensive. In contrast, the extrinsic method involving the in vivo change of physiological and biochemical environment and in vitro surface modification is simpler and more economical. Accumulating research has reported that the change of a single metal ion content and the whole metal ion environment can impart desirable mechanical properties to silk proteins through inducing conformation transition, which will offer a wider application for silk proteins in the traditional textile field at least [16,17].

Silk is known to be very popular in high-quality home products, like clothing, bedding, sofas, and curtains, but its fire risk must be kept as low as possible because the combustion of silk close to the skin will cause severe burns. The modification of silk's flame retardancy has become one of the focuses of research [18,19]. The traditional flame-retardant agents are halogenated compounds, organophosphorus compounds, nitrogen-containing compounds, phosphorus–nitrogen synergistic compounds, and zirconium and titanium metal complexes [18,20]. Unfortunately, these agents have problems with toxicity, environmental persistence, and bioaccumulation [21–23]. Therefore, the development of environmentally friendly and sustainable flame retardancy methods is necessary. The research found that metal salts could hinder the thermal decomposition of polymers during combustion and metal chelates favored the formation of char [18,24]. Considering that silk proteins contain abundant carboxyl, amino, hydroxyl, and amide groups, which can chelate metal ions well, the flame-retardant effect of metal ions on silk fabrics has been investigated [19,25]. The use of metal ions may be an environmentally sound and efficient method to augment the flame retardancy of silk fabrics and a detailed summary can shed light on further study.

According to previous reports, approximately 12% of used chemical dyes enter the sewage effluent, and 20% of this enters nature from the treated sewage effluent [26]. The accumulation of synthetic dyes, mordants, and finishing materials from the textile industry will pose a huge threat to the environment, demonstrating the need to find environmentally sound methods to improve the color fastness of silk. Due to their stable binding to silk, metal ions are found to facilitate the color fastness of silk fibers, and many studies have been conducted to explore this, which may substantially reduce the discharge of synthetic dyes and mordants and offer a new ideal for the dyeing process of silk fibers [27–29].

Apart from the traditional fabric industry, silk has been used in environment remediation as an adsorbent to remove heavy metal ions from contaminated water [30]. Heavy metal pollution in waterbodies has been considered a serious problem because it causes profound harm to the ecosystem and human health due to the high toxicity and persistence of natural degradation [31]. For instance, Cr^{6+} can cause epigastric pain, nausea, and vomiting [32], and prolonged exposure to Cr^{6+} can cause lung cancer [33]. The conventional approaches for the removal of heavy metal from waterbodies primarily involve precipitation by chemical agents, redox reactions, adsorption using activated carbon, electrochemical treatment, ion exchange using resins, solvent extraction, and evaporation [34]. Among them, adsorption is very popular because it has the advantages of high efficiency, easy operation, and wide sources. Due to the contaminated water that remains to be processed containing not only heavy metals, often with low concentration, but also light metal ions, often with high concentration, selective and focused adsorption with high efficiency is challenging. Meanwhile, structural integrity, ion desorption, and no secondary pollution are required. These requirements render ecofriendly and economical adsorbents well warranted [35]. Silk proteins adsorb heavy metal ions through chelation and electrostatic interactions. SF or sericin are often made into films, beads, and particles, or combined with other ecofriendly adsorbent materials using a mild process outlined in studies on their adsorption performances [3,36,37]. The silk-based composite adsorbents not only exhibit

better adsorption efficiency compared to silk, but also maintain the same characteristics as silk, including selective adsorption, durability, and biodegradability [36,38]. This indicates that silk-based composite adsorbents have a great potential for practical application in the treatment of heavy metal ion-contaminated water.

Besides environmental protection and restoration, the biodegradability and tight adsorption of metal ions of silk proteins also open up new applications for them in biosensing. In recent years, metal nanoparticles (NPs) and nanoclusters (NCs) have occupied researchers' attention in biosensing owing to their simple and green synthesis, unique properties, and cell viability [39–41]. Among these metal nanostructures, noble nanostructures are more prominent owing to their special optical properties, hierarchical structure, and catalytic properties [42]. Gold nanostructures can be obtained through simple approaches owing to their stability in aqueous solutions. Nevertheless, other metal nanostructures, including silver nanostructures, are relatively active in aqueous solutions, for instance, silver NPs usually exist as colloids in aqueous solutions [43], and thus, their applications are limited because their optical properties are highly dependent on the size and morphologies [44]. If silver NPs are synthesized in aqueous solutions, stabilizers and redundant processes are required, which also will change the properties of silver NPs [45]. Finding proper solid support where silver ions and other metal ions can be reduced to zero-valent atoms in situ in mild conditions is overwhelmingly difficult. Fortunately, researchers have found that SF is a good template for silver and gold NPs because the tyrosine of SF has reduced reducibility [46–48]. Taking the silver ion as an example, under ultraviolet (UV) light, the phenolic hydroxyl of the tyrosine side chain is oxidized to a carbonyl group, while the silver ion is reduced to a silver atom. Using biocompatible SF as a template and/or a component to fabricate metal nanostructures with specific properties on optics and surface chemistry in situ makes the fabrication more ecofriendly and simpler as well as expands the application to in vivo micro monitors and smart consumer electronics for the observation of food quality and environment [49–52].

Another novel field of application for silk proteins, based on their interaction with metal ions, is electrochemical materials, including energy-storage materials for the preparation of micro batteries to power implantable devices and carbon-based electrocatalytic composite materials for the catalysis of hydrogen evolution reactions (HERs), oxygen evolution reactions (OERs), and oxygen reduction reactions (ORRs) [53,54]. Transient implantable medical bionics offer great possibilities for intelligent controlled release of drugs and tissue regeneration, like wounding healing [55]. Nevertheless, this technology suffers from power systems with controlled biodegradation. Silk proteins, as natural proteins, are a promising material to fabricate implantable micro energy-storage units for bionics because they have tunable biodegradation, minimal immunogenic response to the human body, and can entrap metal ions and active molecules for power supply. Owing to chelation and electrostatic interactions, metal ions can be uniformly deposited on SF-based templates or two-dimensional (2D) and three-dimensional (3D) porous nanostructures. This advantage is also favorable for the fabrication of catalysts, which promote the nucleation of metal NPs on the carboxyl and hydroxyl of SF. Additionally, silk proteins have a high content of nitrogen, and thus other nitrogen sources are no longer needed when preparing N self-doping carbon [56]. The silk-based electrocatalysts are inexpensive, efficient, and stable for HERs and OERs. It has been found that the obtained carbon catalyst exhibited a unique hierarchical porous structure with pores of varying size, exposing more implantation sites for catalytic active metals [57–59].

Based on the above introduction to the effects of metal ions on silk's properties and the emerging application of silk/metal composites, the review aims to elucidate the optimization of silk properties and the expansion of applications based on its interaction with metal ions. The novel applications include heavy metal-contaminated water remediation, silk-based biosensing materials, and silk-based electrochemical materials. The interactions of silk proteins with metal ions, and their properties that contribute to the above novel applications, are also clarified to give a theoretical foundation.

2. Interaction of Silk Proteins with Metal Ions and the Factors Influencing the Interaction

2.1. Amino Acid Composition

Bombyx mori L. silk is composed of SF and sericin, featuring an elliptical cross-section and a diameter of approximately 30 μm (Figure 1A). The SF contains two SF fibers, each of which exhibits a triangular or semi-elliptical shape, with a diameter of roughly 10 μm. In silk, SF comprises 70–80%, while silk sericin accounts for about 20–30% [3,49,60].

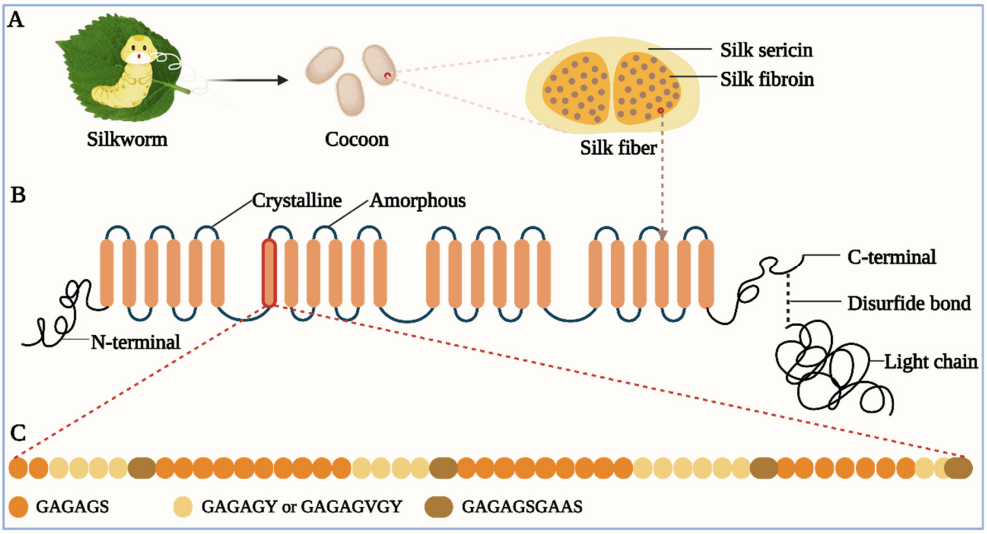

Figure 1. (**A**) Silk components. The silk cocoon is made of silk fibers spun by silkworms. The silk fiber consists of SF and sericin. (**B**) Schematic of H-chain. H-chain has four different domains: crystalline domain, amorphous domain, N-terminal, and C-terminal. H-chain and L-chain are connected by a disulfide bond at the H-chain's C-terminal. (**C**) Amino acid sequence of the crystalline domain. It includes several repetitive polypeptide segments, mainly including GAGAGS, GAGAGY (or GAGAGVGY), and GAGAGSGAAS.

The SF is a macromolecular and fibrous protein comprising three elementary units: a fibroin heavy chain (H-chain), a fibroin light chain (L-chain), and a glycoprotein (P25) [61–63]. The H-chain consists of roughly 5200 amino acid residues, including glycine (45.9%), alanine (30.3%), serine (5.3%), valine (1.8%), and 15 other amino acids. It is composed of four different domains: crystalline domain, amorphous domain, N-terminal, and C-terminal [64,65]. The crystalline domain primarily consists of several repetitive polypeptide segments, of which two hexapeptides (Gly-Ala-Gly-Ala-Gly-Ser (GAGAGS) and Gly-Ala-Gly-Ala-Gly-Tyr (GAGAGY)) account for approximately 70%, simplifying the amino acid sequence of the crystalline domain (Figure 1B,C) [66,67]. The crystalline domain and amorphous domain alternate within the H-chain. The L-chain has no repetitive polypeptide segments and is predominantly composed of alanine and aspartic acid. The H-chain and L-chain are connected by a disulfide bond between Cys-c20 (the cysteine residue located at the 20th position from the C-terminal of the H-chain) and Cys-172 of the L-chain [68]. The bond is crucial for fibroin's normal secretion from the posterior silk gland. Without it, the secretion of SF will be impeded [69,70]. The dominant crystal structure of natural SF constitutes Silk I and Silk II [71,72]. The Silk II is an antiparallel β-sheet structure and is a stable crystal structure due to the powerful hydrogen bond between neighboring peptide blocks, which imparts excellent mechanical performances such as high tensile strength and toughness to SF [71,72]. Like SF, sericin is also a macromolecular protein. However, it is globular and usually discarded during the silk degumming process [73,74]. It envelopes SF like glue, cementing two SF fibers together into SF, and facilitating the flow of SF in silkworms [75,76]. Silk sericin is generally believed to constitute 18 amino acids, among which the two most abundant amino acids are aspartic acid and serine, which account for approximately 33.4% and 16.7%, respectively [77,78].

The amino acid composition of SF and sericin set the basis for the interaction of silk proteins with metal ions. For one thing, the oxygen atom of carboxyl groups and the nitrogen atom of amino groups in amino acids contain lone pairs of electrons. After dehydration condensation, the oxygen atom and nitrogen atom in amide groups can coordinate with metal ions. In addition, the terminal carboxyl groups, terminal amino groups, and some groups in the side chains of amino acid residues (like the hydroxyl of sericin [79,80]) can also adsorb metal ions through coordination. Furthermore, silk proteins possess amphoteric behavior. When the pH of a solution exceeds its isoelectric point (3.6–5.2 [81,82]), it releases protons, becoming negatively charged, and therefore it can bind with metal ions electrostatically.

2.2. Interaction of Silk Proteins with Metal Ions

The bond between animal proteins and metal ions deeply affects the function and application of animal proteins. The interaction of silk proteins with metal ions includes electrostatic interaction and chelation [34,35,83–85]. The electrostatic interaction is generally the ionic interaction between the negatively charged functional groups of silk proteins and positively charged metal ions. The silk proteins possess abundant polar functional groups with a negative charge, which include -COOH, -NH_2, -OH, -CO-NH-, -CO-, and -S-S- [86,87]. These negatively charged functional groups provide binding sites for metal ions. In addition, these polar functional groups contain atoms with lone pairs of electrons, including O and N [54,88,89]. These atoms are prone to chelate with electron-deficient metal ions, forming coordinate bonds. The electrostatic interaction and chelation impart a strong affinity for metal ions to silk proteins. The preferential interactions of an SF peptide and two artificial peptides (RLWRLLWRLWRRLWRLLR (C6M1) and RLLRLLLRLWRRLLRLLR (C6)) with Cu^{2+} than anthocyanin and the resulting protective effect on anthocyanin set excellent examples [90–92].

The formation of silk/metal composites usually results from the combined effect of these two interactions, which can be demonstrated with the following examples. In an ultrafiltration experiment using sericin biopolymer, the removal efficiencies of five metal ions (Pb^{2+}, Co^{2+}, Ni^{2+}, Cu^{2+}, and Zn^{2+}) increased, and their permeate fluxes decreased with increasing sericin dose at neutral pH before reaching a plateau [83]. This was attributed to the higher availability of anionic reactive sites and more atoms containing lone pairs of electrons with increasing sericin dose, leading to more metal ions forming complexes with sericin. The chelation reaction between divalent metal ions and poly dentate ligands (PDLs) of sericin (S), such as NH_2-, -S-S-, and -COOH, can be written as Equation (1). Furthermore, this study found that -NH_2 was very effective in promoting metal ion binding to sericin and served as an example for illustrating chelation (Figure 2A). Stable sericin/metal complexes were formed due to abundant active amino groups chelating with metal ions. The structure of the active amino groups changed with pH: -NH_2 tended to be deprotonated at basic pH, making sericin negatively charged, while it tended to be protonated at an acidic pH, making sericin positively charged. In addition, each bivalent metal ion chelated with four -NH_2. This illustration of sericin's charge is consistent with a study in which silk microparticles were used to adsorb Cr^{6+} in aqueous solutions [93]. The study found that the net charge of sericin was positive at pH 1–2. The reason was that the isoelectric pH of sericin was approximately 4.0 due to carrying more acidic amino acid residues, for example, glutamate acid and aspartic acid, than basic amino acid residues [82,94]. The dominant existing forms of Cr^{6+} were H_2CrO_4, $HCrO_4^-$, and $Cr_2O_4^{2-}$ at pH below 1, 2–6, and above 6, respectively [95]. At pH 1–2, owing to the electrostatic interaction of the negative metal ions with the positively charged sericin, sericin microparticles adsorbed Cr^{6+} effectively and the adsorption capacity exhibited a downward trend as pH increased from 1 to 5. Note that the study reflects that although sericin still interacted with metal ions due to a combination of electrostatic interaction and chelation, the charge of the substance participating in the binding and the binding site could be different and varied with reaction parameters, such as pH and the properties of metal ions. Another study also demonstrated that the interaction between sericin and metal ions was dominated by chelation and electrostatic interaction

between sericin's active amino groups and metal ions (Figure 2B) [96]. Due to the stronger chelation and electrostatic interaction between sericin and metal ions, metal ions in aqueous solutions first interacted with sericin and then with anthocyanin, making anthocyanin a suitable indicator for the saturation state of adsorption for the filter membrane. Due to the formation of coordinate bonds, the adsorption using silk proteins was mainly chemical and follows a pseudo-second-order kinetic model [93,97–99].

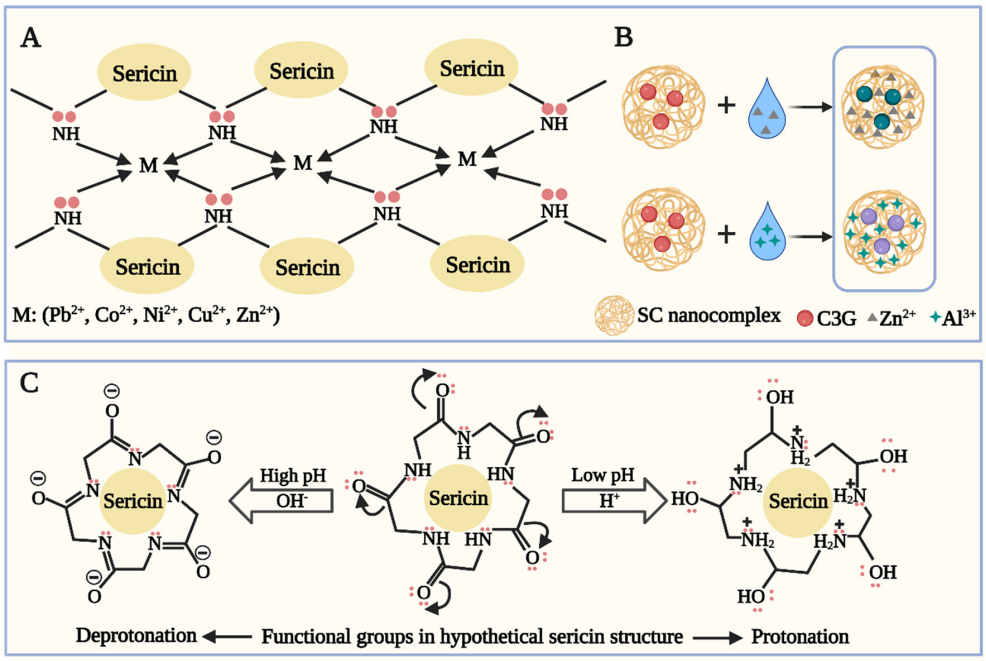

Figure 2. (**A**) Sericin/metal complex between metal ions and sericin's active amino groups. Adapted with permission from ref. [83]. Copyright 2014, Elsevier. (**B**) Binding between sericin/anthocyanin (SC) nanocomplex and Zn^{2+} and Al^{3+}. Due to anthocyanin's different color changes after chelating with different metal ions, anthocyanin is a suitable indicator for the saturation state of adsorption for the filter membrane. Adapted with permission from ref. [96]. Copyright 2022, The Royal Society of Chemistry. (**C**) Potential protonation and deprotonation processes at acidic and alkaline pH of sericin. Both protonation and deprotonation are assumed to occur at active amino groups. Adapted with permission from ref. [83]. Copyright 2014, Elsevier.

Metal-Sericin Complexation:

$$Pb^{2+}/Co^{2+}/Ni^{2+}/Cu^{2+}/Zn^{2+}(aq) + n[PDL(S)]^{2-}(aq) \rightarrow [Pb/Co/Ni/Cu/Zn\text{-}PDL(S)_n](aq) \quad (1)$$

where PDL is short for poly dentate ligand, and S is short for sericin.

2.3. Factors Influencing the Interaction of Silk Proteins with Metal Ions

Several factors influence the interaction of silk proteins with metal ions, such as pH, contact time [93], temperature [34,97], and metal ion properties [97,100–102] (Figure 3).

pH plays a crucial role in the chemical formula (partially due to pronation and deprotonation (Figure 2C) and the surface charges of sericin and metal ions. Therefore, pH is the main influencing factor for the adsorption of metal ions by sericin [93,103]. The adsorption capability is a function of contact time, which can be employed to determine the adsorption kinetic model. Throughout the adsorption process, the adsorption capability of a sericin-based adsorbent typically exhibits a rapid increase, followed by a gradual increase before reaching a plateau. The plateau signifies that the adsorption of metal ions is saturated because active sites are no longer available in the adsorbent materials [93]. The equilibrium time is defined as the duration of the adsorption process, while the maximum or saturated adsorption capacity refers to the amount of adsorbed metal ions. In practical applications, contact time affects the

cost-efficiency of adsorbents for metal ions. Temperature is another critical factor influencing the interaction mechanism between metal ions and silk proteins. The adsorption can be classified as either endothermic or exothermic, based on the variation of metal ion adsorption capacity with temperature. If the capacity increases with rising temperature, the adsorption is endothermic, and vice versa. The binding-free energy for silk proteins to different metal ions primarily pertains to the properties of metal ions, including charge-accepting ability, ionic radius, and valence state. The electrostatic interaction between the negatively charged ligands in silk proteins and metal ions, as well as the charge–dipole interaction between metal ions and noncharged ligands in silk proteins, is stronger when metal ions carry a higher net charge. For groups IA and IIA, a larger ionic radius results in a smaller charge density, endowing ions with lower electronegativity and subsequently reducing their affinity to silk proteins. However, this rule does not apply to groups IB and IIB due to significant relativistic effects [104]. For groups IB and IIB, although the ion with a larger radius has a smaller charge density, the relativistic effect leads to a strong stabilization of the vacuum 6s orbital, which enhances the charge-accepting ability and thus its interaction with negatively charged ligands. For instance, Hg^{2+} and Au^{+} had a stronger charge-accepting ability than Zn^{2+} and Ag^{+} that belong to the same groups in the periodic table, respectively. When two metal ions have similar valence states and radii, the one with a stronger charge-accepting capability demonstrates a greater affinity to silk proteins and forms a more stable silk protein/metal complex than the other, for which the interactions of sericin with Mg^{2+} and Zn^{2+} set a good example [104].

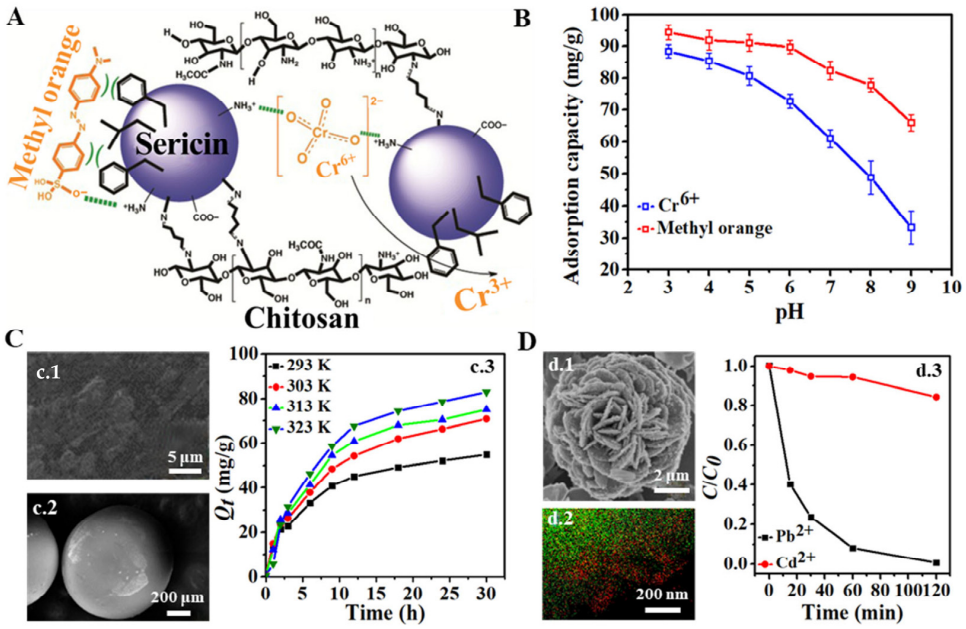

Figure 3. (**A**) Possible interactions between the chitosan/sericin conjugate and methyl orange dye and Cr^{6+} ions, and reduction of Cr^{6+} to Cr^{3+}. Hydrophobic interactions are represented by ") (", "electrostatic" is represented by the green dashed line. (**B**) Influence of pH on the coadsorption of Cr^{6+} ions and methyl orange dye using a chitosan/sericin conjugate. Adapted with permission from ref. [36]. Copyright 2018, The Royal Society of Chemistry. (**C**) (**c.1**,**c.2**) Field emission scanning electron microscopy (FE-SEM) images of sericin/kraft lignin beads after Cr^{6+} adsorption. (**c.3**) Kinetics curves of Cr^{6+} adsorption by sericin/kraft lignin blend beads at 293, 303, 313, and 323 K. Adapted with permission from ref. [97]. Copyright 2016, Kwak et al. (**D**) (**d.1**) SEM images showing the unique growth of uniformly distributed needle-shaped nanowires with an initial Pb^{2+} concentration of 15 mg/L. (**d.2**) Scanning transmission electron microscopy-energy dispersive X-ray spectroscopy (STEM-EDX) mapping indicates the formation of Pb nanowires (Green, Cu; Red, Pb). (**d.3**) Adsorption rate showing the selective adsorption of Pb^{2+} in the presence of Ca^{2+} ions. (C and C_0 are the metal ion concentrations before and after adsorption). Adapted with permission from ref. [105]. Copyright 2016, American Chemical Society.

3. Favorable Properties of Silk Proteins for Application Expansion

3.1. Biocompatibility

The use of pristine silk-based biomaterials in surgeries or in vivo studies will likely trigger an inflammatory response, allergy, and immunogenicity [106]. However, SF, obtained by completely removing the sericin layer from pristine silk using the degumming process, causes a minimal immunogenic reaction, which lays the foundation for their increasing applications in biomaterials [107–109]. In a study, SF was used as a bridging agent to self-assemble 2D MXene nanosheets into a continuous wave-shaped lamellar macrostructure, which endowed the obtained SF/$Ti_3C_2T_x$ MXene films with good biocompatibility [110]. Results showed that these films had a good viability (99.5% $\pm$ 0.8% after 144 h) for human skin fibroblast-HSAS cells in a cytotoxicity test, and therefore were safe for subcutaneous implantation. Similarly, SF was used to enhance the biocompatibility and biodegradability of the designed multifunctional biocomposite scaffold in another study [111]. Results showed that the obtained SF, cellulose, and β-cyclodextrin-based hydrogel modified by magnetic copper-doped cobalt ferrite ($CuCoFe_2O_4$) had a cell viability of 84.74% after three days and 80.55% after seven days in an MTT (3-(4,5)-dimethylthiahiazo (-z-y1)-3,5-di-phenytetrazoliumromide) assay using Hu02 cells, and there was no significant difference in statistical analysis between it and untreated cells. Its hemolytic effect was also low (below 3%). Therefore, this hydrogel had good biocompatibility.

The previous comparative tests between pristine silk and sericin-free silk speculated that it was sericin that triggered the immunoreaction [112–114]. However, sericin by itself has been observed to cause minimal immune responses [115,116]. It can promote the migration of fibroblast at a concentration of 100 μg/mL in vitro scratch assays, shortening the wound length, and ameliorates the re-epithelialization of a burned surface and its complete healing in a clinical study, without any infection or severe immune reaction [117]. Sericin has almost no adverse effects on the viability of NCM460 cells (94.8%) at a concentration of 100 μg/mL after 48 h co-incubation and the encapsulation by it can greatly increase the cell viability of caffeic acid [118]. Furthermore, a study demonstrated the similarity of immunogenicity between SF and sericin because after being implanted subcutaneously into ten Sprague-Dawley rats for nearly five months, the pristine silk and SF did not induce any infection or other anomalies, the surgical wounds healed well, and a mass of connective tissue wrapped the implants [119]. The immune reaction reported in previous studies may pertain to sericin's dose and molecular weight because the collagen–SF–sericin scaffolds show no evident inhibitory effect on the proliferation, attachment, and spreading of fibroblast cells, and low-molecular-weight sericin at a concentration of 1 mg/mL shows great cell viability for fibroblast and macrophages and human adipose stem cells [115,120,121].

3.2. Biodegradability

Biodegradability is another important property that enables new uses for silk proteins. Silk is degraded mainly by enzymatic activity. Since it is composed of amino acids, silk proteins will be degraded into soluble peptides and free amino acids, which do not cause environmental pressure and can be absorbed in in vivo studies. The enzymes used for the degradation of silk proteins involve various proteases (like protease XIV, chymotrypsin, carboxylase, and lysozyme [122]). The protease acts on the surface of silk materials, reduces the hydrophilic segments in the structure, and progressively removes the β-sheet structure in silk proteins. The degradation by protease XIV occurs on both the crystalline and amorphous domains [123,124].

The degradation of silk proteins is affected by numerous factors, including temperature, processing method, structure, porosity, SF concentration, etc. [123,125–129]. In a study, after 21 days of degradation, as the SF content increased from 21.3% to 44.8%, the weight loss of porous SF/cellulose nanofibril sponges increased from 15.4% to 19.1% in phosphate-buffered saline (PBS) solution and from 29.3% to 44.0% in protease XIV solution [130]. In another study, the degradation rate of a silk I scaffold was different after different post-treatments

including ethanol and high-temperature/high-pressure, which might have resulted from the crystallinity variation and the formation of a few β-sheet crystals [131].

The degradation rate of silk proteins is often evaluated via mass loss, mechanical properties, morphology variation, and molecular weight [124,132–134]. In a study, the mass of milled silk particles reduced rapidly to 40%, the volume median particle size decreased from 6.4 to 1.8 µm after 12 days, and the morphological changes in silk particles and fibers were analyzed using SEM, based on which, a model reflecting the degradation mechanism of milled silk particles was established [124]. Another study reported that the native and PEGylated silk NPs had a mass loss of 60% and 40%, respectively, of the original mass, increased size, and reduced amorphous content in the silk secondary structure [135].

3.3. Mechanical Property and Processability

Bombyx mori L. silk exhibits an ultimate tensile strength of 740 MPa and a modulus of 10 GPa. Its breaking strain is 20% and the Young's modulus is 4.53–57.11 GPa [136,137]. The mechanical property of SF differs from *Bombyx mori* L. silk slightly due to the removal of sericin. The comparison among pristine silk, SF, and several other natural polymers demonstrates that pristine silk and SF possess higher tensile strengths [136,138,139]. To obtain the desired mechanical properties for better applications, silk proteins can be modified using different methods, including processing technologies, solvent composition, temperature, and molecular weight [140–143]. Specifically, as the molecular weight of sericin increased, the gel strength increased, and the bending strength and bending strain of the sericin sponge remarkably increased in both dry and wet states [143]. Another study found that the SF hydrogel made based on the conformation transition induced by hexafluoroisopropanol and deionized water, in turn, possessed a Young's modulus of 6.5 ± 0.2 MPa, ten to hundred times higher than that of the conventional hydrogel (0.01–1 MPa) [144,145].

Besides biocompatibility and biodegradability, the unique physical and chemical structures impart silk proteins with versatile processability [146,147]. Extensive literature indicates that silk can be processed into various shapes, including films, hydrogels, sponges, microparticles, and microneedles [5,148–152]. A smart microneedle for glucose-responsive insulin delivery was created by SF and phenylboronic acid/acrylamide. After optimization, the needle region was made by SF and phenylboronic acid/acrylamide, and the base layer was made by SF. This microneedle enabled insulin release in a way corresponding to the insulin's change [5]. Another study prepared SF NPs with a diameter of 229–2286 nm and load efficiency of 22–40% using emulsification. The smaller NPs (with a diameter of about 200 nm) showed a shorter plasma circulation time and greater maximum plasma concentration than the larger NPs (with a diameter of about 800 nm).

4. Application Based on the Interaction between Silk Proteins and Metal Ions

The interaction of silk proteins with metal ions and their outstanding properties not only enhances their applications in the conventional textile industry, but also ushers in novel applications in environmental remediation, bioengineering, and electrochemistry [18,153,154].

4.1. Performance Optimization of Silk Fabric

Silk textiles have been used in China for nearly four thousand years, though they are plagued with unsatisfactory mechanical properties and flammability [1,2]. To solve these problems, much work has been carried out, finding the binding of metal ions with silk proteins enabled the optimization of mechanical properties and the improvement of flame retardancy and color fastness [19,25].

4.1.1. Mechanical Property Optimization

The silk fibers' mechanical properties pertain to the metal ion environment in silk glands, especially in the anterior gland. A study reported that the content of metal ions in the anterior silk gland is higher than that in both the middle and posterior silk glands, and a specific metal ion environment in the anterior silk gland is kept for the silk proteins'

transport and conformational transition [155]. In another study, the silk fibers' mechanical properties were improved by genetically interrupting the ionic environment for silk formation (Figure 4A) [16]. As silks' Ca^{2+} content decreased due to overexpressing endoplasmic reticulum Ca^{2+}-ATPase (an ion-transporting protein) in the anterior silk gland, more β-sheet and α-helix structures were observed, and the silk fibers' tenacity and extension increased noticeably. The study was an in vivo demonstration of the relationship between metal ion content and silk fibers' mechanical properties.

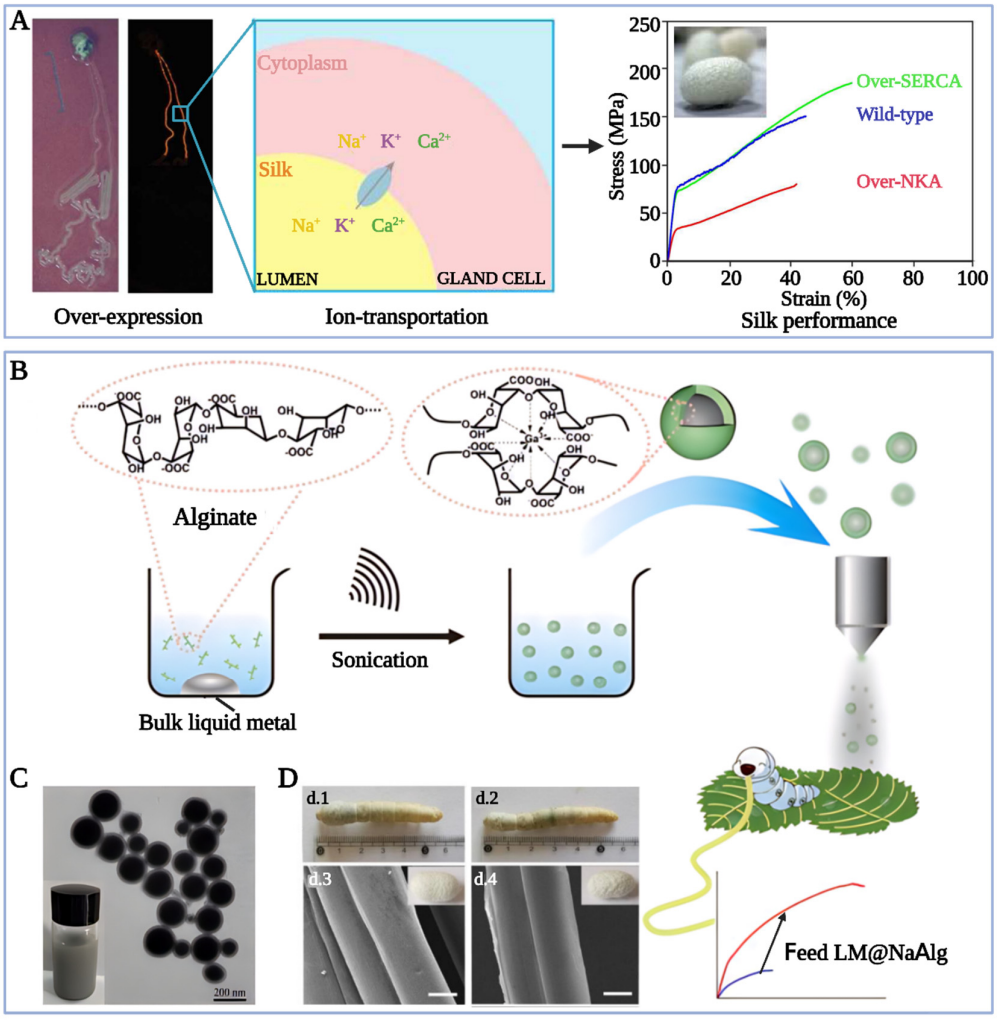

Figure 4. (**A**) Red fluorescence only detected in the anterior silk gland of *BmCP231* (an anterior silk gland-specific promoter) transgenic silkworm under a red fluorescent protein-excitation wavelength light. Schematic of ion transportation from silks to gland cells, and a comparison of the stress-strain of Over-NKA (red), Over-SERCA (green) and WT (blue) silk fibers (NKA and SERCA are the silkworm's Na^+/K^+-ATPase α subunit (*BmNKA*α) and endoplasmic reticulum Ca^{2+}-ATPase, respectively, and WT is wild-type). Adapted with permission from ref. [16]. Copyright 2015, American Chemical Society. (**B**) Schematic illustration of the sonicating liquid metal in the alginate solution and the liquid metal nanodroplets shelled in the alginate microgel. (**C**) Transmission electron microscopy (TEM) image of the LM/NaAlg nanodroplets. (**D**) (**d.1**,**d.2**) Photographs of the mature larvae fed with control diet and LM/NaAlg-2 diet, respectively. (**d.3**,**d.4**) SEM images showing the morphology of the degummed silk fibers and the cocoons of the mature larvae fed with the control diet and LM/NaAlg-2 diet, respectively. Adapted with permission from ref. [156]. Copyright 2022, Gao et al.

The silk fibers' mechanical properties can be optimized through an in situ changing the metal ion environment through feeding or injecting metal ions into silkworms. The silk fibers spun by silkworms fed with Ca^{2+} and PO_4^{3-} had more α-helix and random coil

structures and fewer β-sheet structures, leading to higher fracture strength, elongation, and toughness modulus [8]. The mechanical properties of silk fibers spun by silkworms fed with liquid metal alginate-coated NPs (LM/NaAlg) were greatly improved, with a breaking strength of 814 MPa and a breaking elongation of up to 70% (Figure 4B–D) [156]. Characterization results indicated that LM/NaAlg perfectly combined with the silk fibers spun by these silkworms and LM/NaAlg hindered the conformation transition of SF from the random coil and α-helix structure to the β-sheet structure by forming hydrogen bonds between LM/NaAlg and SF. Moreover, silk fibers spun by silkworms that were fed or injected with ethylenediaminetetraacetic acid (EDTA), a strong metal chelating agent [157,158], in their fifth instar larvae exhibited a significant conformational transition from β-sheet structure to β-turn structure and their strength, toughness, and Young's modulus decreased greatly [11].

Additionally, silk fibers notably shrunk and curled after being treated with neutral calcium salts (e.g., $CaCl_2$) at specific concentrations, leading to the development of elastic silk materials [159,160]. The shrinkage and curling occur because Ca^{2+} chelates with fibroin at the -OH of the serine side chain and the tyrosine side chain of SF macromolecular chains. This coordination disrupts some hydrogen bonds and Van der Waals force between fibroin peptide chains, causing fibroin protein molecules to rearrange, altering the orientation of the original stretched fibroin macromolecular chain. These results indicate that silk fibers' mechanical properties can be modified through in vivo changing the metal ion environment and in vitro metal ion treatment.

4.1.2. Flame Retardancy Enhancement

The enhancement of the flame retardancy of silk fibers with metal ions, resulting in an extended lifetime and reduced fire risk, has been demonstrated in many investigations [18,156,161–163]. After being immersed in Fe^{3+}, Al^{3+}, and Ti^{4+} solutions, silk fabrics had a suppressed smoke generation, an increased limiting oxygen index (LOI) with increasing metal ions concentrations, and an increased char length with increasing washing cycles, indicating that both fire retardancy and washing resistance were improved by metal ions (Figure 5A) [18]. The inflated structure features of char residues were consistent with the typical intumescent fire-retardant effect. Another reason is that the binding sites between metal ions and peptide chains are usually the carbonyl and amino of side chains near specific amino acid residues, like tyrosine residues. This binding seizes the excitation energy required for free carbonyl formation from tyrosine residues, thus preventing the breakage of peptide chains. Further, silk fabrics treated with casein phosphopeptide-ferrous salt (CPP-Fe^{2+}) and casein phosphopeptide-titanium salt (CPP-Ti^{2+}) exhibited a good, durable flame-retardant capability, with an LOI of 27.8% and 28.0%, respectively, and a residual char length of less 15 cm after 20 washes. In addition, the CPP-Fe^{2+} treated fabrics also exhibited a brilliant yellow color and a good rubbing fastness (Figure 5B–D) [164]. Likewise, silk fabrics treated with three flavonoids (baicalin, quercetin, and rutin) and two metal ions (Fe^{2+} and Ti^{4+}) possessed a good char-formation capacity, leading to a flame-retardant capacity and smoke suppression, and antibacterial and antioxidant abilities [19]. Their color fastness and rubbing fastness were enhanced with the mordanting treatments because coordination bonds were formed among silk fibers, metal ions, and flavonoids. These performances remained almost unchanged even after 20 washes. A further study of ref. [164] manifested that silk fabrics treated with 20% tannic acid and 2 g/L ferrous salt exhibited excellent flame retardant capability, antibacterial ability, and washing durability [25]. The fabric's LOI rose from 23.6% to 27.5%, the antibacterial rate rose from 22% to 95%, and the length reduced from 30.0 cm to 11.2 cm. These performances remained almost the same as before being washed even after 20 washes.

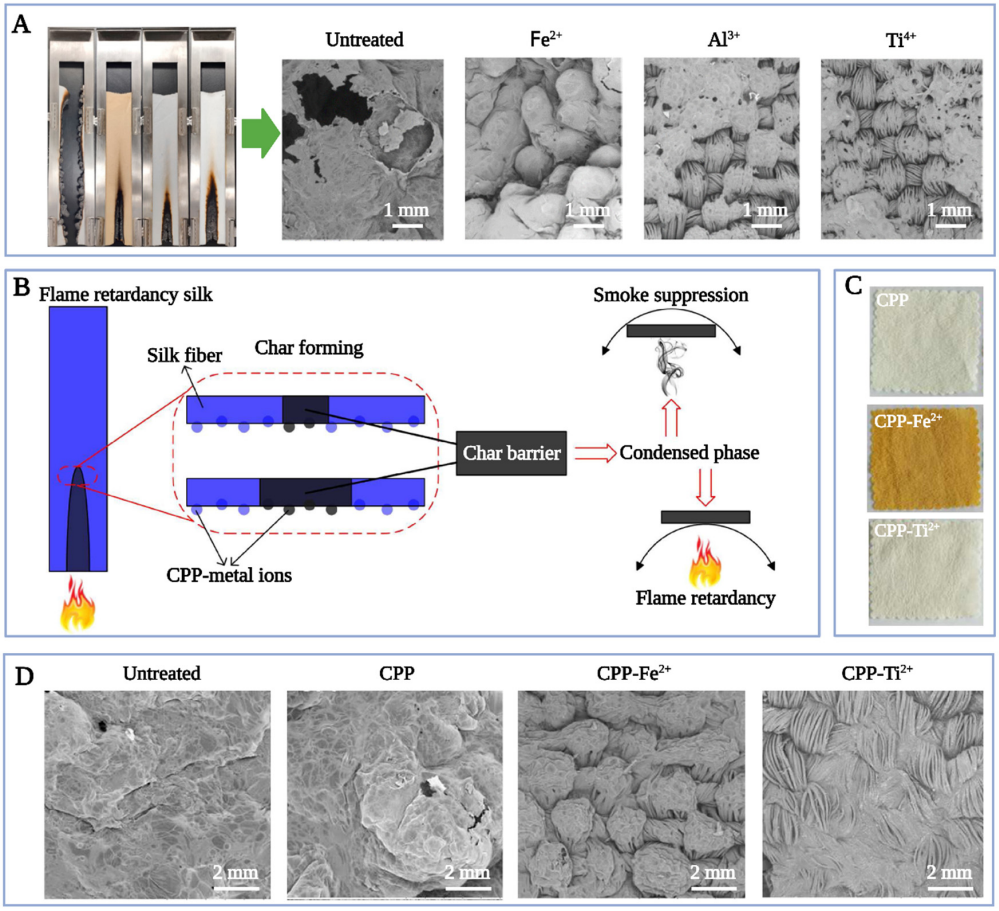

Figure 5. (**A**) Images of the treated silk fabrics and the SEM images of silk char residues after vertical burning. Adapted with permission from ref. [18]. Copyright 2020, Elsevier. (**B**) Flame-retardant mechanism of CPP-metal ions treated silk fabrics. (**C**) Colorimetric characteristics of silk fabrics treated with 10 g/L CPP and 4 g/L metal salts. (**D**) Morphological structures of charred products from vertical burning. Adapted with permission from ref. [164]. Copyright 2019, Elsevier.

4.1.3. Color Fastness Improvement

The improvement of the color fastness of silk fibers with metal ions is mainly due to the chelation between silk proteins and metal ions. The coordinate bonds formed between the polar functional groups (e.g., -NH_2 and -OH) of silk proteins and metal ions can induce the conformational transition of silk peptides [165], which can change the available combination site between dyes and silk fibers (i.e., dye site). In addition, the conformational transition from the random coil (Silk I) to β-sheet can create a relatively stable solution environment, and thus enhance the combination between fibroin protein and dyes [166–168]. In a study, silk fabrics were mordanted with two metallic mordants ($SnCl_4$ and $CuSO_4$) and three natural mordants (tannic acid, pinecone, and lemon peel) and were dyed with the dye extracted from spent coffee grounds [27]. Three mordanting methods were used, including pre-, meta-, and post-mordanting. Results showed that metallic mordants led to higher color strength than natural mordants, and the dyed silk fabrics with all mordants exhibited appropriate color fastness to light and washing, especially under the post-mordanting method. Additionally, silk fabrics, dyed with dopamine with the help of Fe^{3+} and sodium perborate oxidant, possessed improved light fastness (Level 4) and an improved anti-UV property with a UV protection factor greater than 30 and UVA < 4%. Its hydrophobicity and weft-breaking strength were better than the pristine silk fabrics. Fe^{3+} acted as the catalyst of the oxidation polymerization of dopamine and the bridge between dopamine and fibers [169].

In addition to the improvement of mechanical properties, flame retardancy, and color fastness, binding with metal ions also can improve silk fabrics' anti-UV, antibacterial, antioxidant

properties, etc. [170–175]. For instance, in another study, multifunctional silk fabric was created by coating polydopamine on the silk fabric's surface and then treating the polydopamine-coated fabric with $FeSO_4$ [170]. The results showed that the Fe^{2+} treated silk fabric had a much higher UV protection factor (38.77%) than untreated silk fabric (3.84%). Anti-infection and osteogenesis are vital for successful bone defect repair. In a study, a synthetic bone grafting material, polyetheretherketone (PEEK), was coated with the SP that contained CuO microspheres and Ag nanoparticles to reduce inherent bioinertness [171]. Under a physiological environment (pH 7.4), the SP released Cu^{2+} and Ag^{+}, promoting the production of alkaline phosphate, collagen, and NO and the Ca^{2+} deposition. An in vivo study showed the PEEK that was coated with the SP containing CuO microspheres and Ag nanoparticles had the largest new bone volume compared to uncoated PEEK and CuO-coated PEEK. To sum up, metal ion treatment will impart novel applications to silk fabrics.

4.2. Heavy Metal-Contaminated Water Remediation

Due to the strong chelation between metal ions and silk proteins, and the biodegradable and inexpensive nature of silk proteins, they can be employed to remove heavy metal ions (like Cr^{6+} and Pb^{2+}) from water [64]. The potential application of silk proteins in heavy metal-contaminated water remediation has been widely studied (Table 1).

Table 1. Metal ions removal in aqueous solutions by employing silk protein-based biomaterials.

Precursor Material	Biomaterial Form	Adsorbate	Adsorption Parameter	Adsorption Property	Ref.
Sericin, copper phosphate	Powder for batch method and film for continuous method	Pb^{2+}, Cd^{2+}, and Hg^{2+}	Sericin concentration (0.01, 0.1, and 1 mg/mL)	• Powders with 1 mg/L sericin reached saturate adsorption within the least time; • Adsorption capacity: 75.3% for Pb^{2+}, 64.3% for Cd^{2+}, and 99.8% for Hg^{2+} with 1 mg/L sericin; • High selectivity for Pb^{2+} (vs. Ca^{2+}).	[105]
SF, cellulose acetate (CA)	Nanofibrous membrane	Cu^{2+}	CA content, Cu^{2+} concentration, and running time	• Adsorption peaked at 22.8 mg/g with 20% CA; • Adsorption rose sharply in 1 h and reached equilibrium at ca. 2 h; • Adsorption rose with Cu^{2+} concentration but the rising rate declined gradually.	[34]
Sericin and medium molecular weight chitosan	Powder for batch method	Cr^{6+} and methyl orange dye	Initial adsorbate concentration, contact time, pH, co-ion, and ionic strength	• Adsorption capacity rose with increasing initial adsorbate concentration, contact time, and chitosan/sericin conjugate dosage, and declined with increasing pH and ionic strength; • No significant effect of the four anions.	[36]
Sericin and kraft lignin	Bead	Cr^{6+}	Blend ratio, pH, initial Cr^{6+} concentration	• Adsorption capacity rose with increasing blend ratio when the ratio was $\leq$50:50; • Adsorption capacity peaked at 68.42 mg/g and then declined with increasing pH, and rose with increasing initial Cr^{6+} concentration and temperature; • Adsorption was controlled by pseudo-second-order kinetic and Freundlich isotherm was the best; • Adsorption capability remained at 50–60 mg/g during seven recycles.	[97]

Table 1. *Cont.*

Precursor Material	Biomaterial Form	Adsorbate	Adsorption Parameter	Adsorption Property	Ref.
Sericin	Microparticle	Cr^{6+}	pH and contact time	• Adsorption capacity peaked at pH 2 and then declined with increasing pH; • Adsorption rate rose rapidly and peaked for ca. 24 h and removal efficiency rose with increasing sericin dosage; • Adsorption was controlled by pseudo-second-order kinetic and Brunauer–Emmett–Teller (BET) isotherm was the best.	[93]
SF, chitosan, and starch	Film	Cr^{6+}	Contact time, pH, adsorbent dosage,	• Removal efficiency rose with increasing contact time and adsorbent dosage, varied with pH, and peaked at ca. 72% at pH 5.5; • Adsorption was controlled by pseudo-second-order kinetic, and Freundlich isotherm was the best.	[176]
SF and wool keratose (WK)	Membrane	Cu^{2+}	-	• WK/SF blend membrane had a higher Cu^{2+} adsorption capability (2.88 μm/mg) than the other three membranes; • Removal efficiency remained at over 90% during six cycles.	[177]
SF and wool keratose	Mat	Cu^{2+}	WK/SF blend ratio and pH	• Adsorption capacity rose with increasing pH (4.5–8.5); • Blend ratio had no significant effect on the adsorption ability.	[178]
SF	Powder	U^{6+} and Th^{4+}	pH, contact time, temperature	• The adsorption ability of U^{6+} rose with pH and that of Th^{4+} peaked at pH 3; • U^{6+} and Th^{4+} adsorption capacities reached the equilibrium within 24 h; • U^{6+} adsorption capacity at pH 6 declined with temperature, but that of Th^{4+} at pH 3 rose with temperature.	[179]
SF	Powder	Th^{4+}	pH, initial Th^{4+} concentration, SF dosage, solution volume, co-ion, retention time, and temperature	• Distribution coefficients and adsorption yield peaked at 84.42% at pH 4 and rose with decreasing initial Th^{4+} concentration, increasing SF dosage and solution volume; • Adsorption yield reached 69.41% in the first seven minutes; • Th^{4+} adsorption was reduced by Ce^{3+} and Fe^{3+} and competed with Sr^{2+} adsorption, and Langmuir isotherm was the best.	[180]
SF and nylon-6	Nanofiber membrane	Cu^{2+}	pH, membrane number, flow rate, and initial Cu^{2+} concentration	• Adsorption capacity peaked at pH 5, rose with increasing membrane number, increasing initial Cu^{2+} concentration before 30 ppm, and decreasing flow rate; • Adsorption capacity in the bath method was higher than that in the continuous method.	[181]

Table 1. *Cont.*

Precursor Material	Biomaterial Form	Adsorbate	Adsorption Parameter	Adsorption Property	Ref.
Sericin and anthocyanin	Film (coating)	Zn^{2+}, Al^{3+}, and Cd^{2+}	Sericin dosage, adsorbate concentration, contact time, temperature, and co-ion	• Sericin/anthocyanin (SC) composites and films could indicate the saturation state of Zn^{2+} and Al^{3+} adsorption; • SC composites have metal ion selectivity but the anti-interference stability needs to be improved; • Zn^{2+} adsorption conformed to both pseudo-first-order and pseudo-second-order kinetics and Freundlich isotherm was the best.	[96]

A 3D flower-like hierarchical biohybrid structure was fabricated using sericin, copper sulfate, and PBS (Figure 6A,B) [105]. The strong chelation of the amide backbone and sericin's polar side chains with metal ions led to kinetically controlled growth of the flower's thin petals in the early growth stage. The subsequent experiment found the fabricated biohybrid flowers had a large BET surface area, and due to these results plus the surface polar functional groups of sericin, the flowers exhibited superior adsorptions of Pb^{2+}, Cd^{2+}, and Hg^{2+} in both batch filtration and continuous filtering process. In addition, the fabricated flower demonstrated selective adsorption for Pb^{2+} over Ca^{2+}, indicating the sericin-mediated flower compounds were a promising adsorbent for water treatment. The silk fibroin/cellulose acetate (SF/CA)-blend nanofibrous membrane was fabricated by an electrospinning approach and had a higher affinity for Cu^{2+} than its components (Figure 6C,D) [34]. The obtained membrane constituted randomly oriented ultrafine fibers with a diameter of 100–600 nm and displayed improved anti-felting performance after treatment with 100% ethanol. The optimal fibroin content for Cu^{2+} adsorption was 80%, leading to a maximum adsorption capability of 22.8 mg/g. This high value manifested a synthetic effect between SF and CA during Cu^{2+} adsorption. Particularly, in another study, SC nanocomposites were fabricated to visually demonstrate the degree of metal ions adsorbed by sericin [96]. Anthocyanin is a natural pigment and its color changes when interacting with certain metal ions [90,182]. Using Zn^{2+} and Al^{3+} as metal ion models, it was observed that both the SC solution and the filter film coated with SC nanocomposites exhibited a gradual change in color from pink to blue (Zn^{2+}) and violet (Al^{3+}) as the concentration of Zn^{2+} and Al^{3+} increased. The ultraviolet and visible (UV-Vis) adsorption of SC solution exhibited a redshift with increasing metal ion concentration. The change in color of SC solutions and their redshift of UV-Vis adsorption indicated that sericin reacted with metal ions first, followed by anthocyanin once sericin was saturated. The visual color difference occurring at 100 mM Zn^{2+} and 0.1 mM Al^{3+} suggested that SC nanocomposites reached saturation for Zn^{2+} or Al^{3+} adsorption at these concentrations. Furthermore, the adsorption capability of the filter film was significantly improved by the SC nanocomposite coating, with an increased removal efficiency from 22.22% to 93.16% for Zn^{2+} and from 10.46% to 53.97% for Al^{3+}.

Apart from Pb^{2+}, Cd^{2+}, Hg^{2+}, and Cu^{2+}, Cr^{6+} is another representative toxic heavy metal ion produced by chemical-intensive industries, and the adsorption capability of sericin-based structures has been explored. For example, a chitosan/sericin conjugate demonstrated maximum adsorption capabilities for Cr^{6+} and methyl orange dye up to 139 and 385 mg/g, respectively, under specific operation conditions [36]. Cr^{6+} was likely immobilized by chitosan/sericin conjugate through electrostatic interaction and reduced to Cr^{3+} (an oxidation state of Cr with 100–1000 times less toxicity than Cr^{6+} [183]) during the adsorption process. Furthermore, the adsorption capabilities were highly pH dependent. Similarly, sericin/lignin particles prepared by coagulation exhibited a higher Cr^{6+} adsorption capability than sericin particles alone [97]. The maximum adsorption capability occurred at a sericin-to-lignin ratio of 50:50 (*w*/*w*) and followed the Freundlich isotherm. In addition, the recovery of >90% of the adsorbed Cr^{6+} by sericin/lignin particles was achieved in a 1 M NaOH solution. The adsorption–desorption process remained stable for over seven cycles, with a recycling efficiency of 82%. Another sericin-based material, ethanol-precipitated silk sericin was prepared

by the electrospinning approach and exhibited a higher Cr^{6+} adsorption capability than sericin macroparticles [93]. The intra-particle diffusion model simulation indicated that the Cr^{6+} adsorption process roughly involved three stages: instantaneous external surface adsorption, intraparticle diffusion, and near equilibrium.

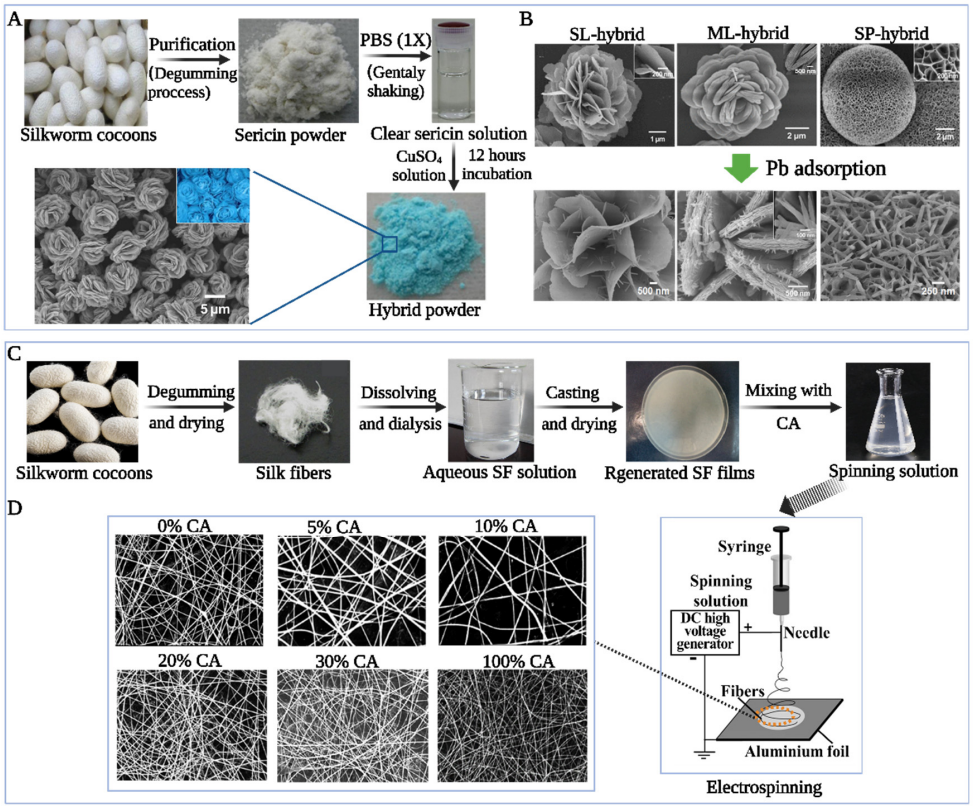

Figure 6. (**A**) Schematic diagram of the preparation of sericin-mediated hierarchical hybrid flowers. (**B**) SEM micrographs of a single hybrid flower before and after Pb^{2+} adsorption. Adapted with permission from ref. [105]. Copyright 2016, American Chemical Society. (**C**) Preparation of silk fibroin/cellulose acetate (SF/CA)-blend nanofibrous membranes. (**D**) SEM micrographs of SF/CA-blend nanofibrous membranes with varying CA contents. Adapted with permission from ref. [34]. Copyright 2011, Springer Nature.

4.3. Silk-Based Biosensing Materials

The use of silk or its derivatives as templates for the synthesis of biosensing materials (e.g., metal NCs) has recently gained increasing interest from researchers for several reasons [46,184–188]. First, silk proteins share common features with often-used protein or peptide templates, such as bovine serum albumin and transferrin [189]). These features involve the possession of abundant functional groups (like -S-, -OH, and -COOH) that can chelate with metal ions, endowing the proteins with an affinity for metal ions and the ability to immobilize on supports [190]. Additionally, silk proteins contain tyrosine and tryptophan, which exhibit reducibility in strong alkaline environments and can reduce metal ions to atoms [191]. Second, silk demonstrates excellent biocompatibility, controllable biodegradability, and outstanding processability [192–194]. Third, as a natural protein fiber, silk fibers are inexpensive compared to synthetic protein fibers and have a simple molecular design [107,195,196]. The practicability of silk-based biosensing materials in biomedical and non-biomedical fields has been widely studied.

4.3.1. Silk/Noble Metal Nanostructure Composites and In Vivo Micro Monitors

Silk-based biomaterials, consisting of silk proteins and other non-immunogenic materials, can be used for biolabeling, bioimage, and real-time, sensitive in vivo monitoring of

analytes in body fluids to realize safer medical treatment and healthcare. Much attention from medical academia has been paid to it [197].

Due to its distinctive optical properties, low cytotoxicity, and small size, the noble metal NC has been a hot spot of research, and its synthesis with biocompatible silk as a template has been studied recently [46,47,198]. For instance, luminescent gold silk was prepared using an in situ method, wherein the silk's surface was coated with luminescent AuNCs [198]. Compared with pristine silk, the gold silk possessed better optical properties, including long-wavelength fluorescence (red), enhanced fluorescence stability (no photobleaching after 30-min UV irradiation), an extended fluorescence lifetime (322 ns), and a larger quantum yield (8%). Additionally, golden silk displayed better mechanical properties, an inhibitory effect on UV light, and high biocompatibility. The X-ray photoelectron spectroscopy measurement revealed that AuNCs combined with silk via Au-S bonds. These results indicated that silk coated with luminescent AuNCs was a promising material for both the textile and biomedical industries, including biosensing, bioimaging, cell adhesion, and tissue engineering. In another study, the in situ growth of AgNCs on SF fibers modified by poly-acrylic acid (PAA) was realized [47]. The in situ synthesis, based on silk fibers, avoided the excessive surface modification and reductant procedures of the synthesis based on bulk materials. Because PAA had abundant carboxylic acid, the binding of Ag^+ to the surface of SF fibers was achieved through the exchange with H^+. Upon exposure to UV light, silver ions were reduced to silver atoms. The prepared SF/AgNCs were proved to be luminescent through UV-Vis adsorption and fluorescent emission measurements. Its emission bond was approximately 550 nm, attributed to Ag_2–Ag_8. Furthermore, the antimicrobial ability of SF/AgNCs against *Staphylococcus aureus* and *Escherichia coli* was demonstrated. The results indicated that SF/AgNCs could be used for biolabeling, specialized fabrics, biosensing, and antimicrobial materials. Similarly, the floriated AgNCs were synthesized using SF fibers as a biotemplate, reductant, and support, at room temperature [46]. The hierarchical morphology of SF fibers provided a large loading surface area and highly uniform metal loading for AgNCs. This study manifested that the SF fiber is a felicitous solid support for in situ synthesizing metal NCs via mild reactions.

In addition to synthesizing noble metal NCs with outstanding optical quality, the fabrication of biosensors and bio-probes was realized for in vivo activity and analyte levels (like biopotential [199], glucose [200], O_2 [148], and antigens [201]), where the silk proteins serve as substrates/superstrates, protective layers, and insulators. Some examples are detailed as follows. A nontransient SF-based bio-interface was fabricated for directly recording various in vivo electrical activity [199]. The study used water-stable SF as a substrate and superstrate to support the electrode construct and was enabled by two key novel concepts: SILK-SEAL (a silk sandwich sensor) and QUICK-SILK (a band-aid to 'paste' the silk devices onto tissue surfaces). The obtained film devices achieved biopotential recordings from the peripheral nerve and the cortex in a rodent stroke model, indicating that the silk sensors could be used as non-dissolvable bio-interfaces in preclinical studies. A biocompatible, cost-effective, and chemically tunable metal–insulator–metal resonator was designed for color filters and superabsorbers using SF and Ag [202]. Results showed that the silk metal–insulator–metal resonator had comparable transmission, adsorption, and quality factor performances to nanostructured plasmonic devices. The absorptive features could be detected even through 1.95 mm thick biological tissue in the first optical window in the tissues (700–900 nm), indicating that this silk resonator could achieve highly sensitive, real-time, and in vivo monitoring for analytes in body fluid.

Further, detecting specific analytes in body fluids using biocompatible devices has been investigated. A flexible biocompatible glucose biosensor chip was fabricated using natural SF as substrate and biocompatible silicone rubber as an encapsulating material (Figure 7A–C) [203]. The Pt working and counter electrodes of the sensor chip were fabricated using thin-film technology, while its Ag/AgCl quasi-reference electrode was fabricated using thick-film technology. The biocompatible glucose biosensor chip had a mean glucose sensitivity of 0.24 ± 0.006 μA/mM in pure PBS, 0.26 ± 0.02 μA/mM in the PBS, to which low-concentration ascorbic acid, noradrenaline, and adrenaline were subsequently spiked, and 0.16 ± 0.01 μA/mM in pure Rigner's solution (pH 7.4), indicating that the biosensor

chip exhibited an acceptable sensitivity and great application potential in real blood samples. In another study, SF and a chromophore, Pd^{2+} tetramethacrylated benzoporphyrin (PdBMAP), were used to synthesize a silk/chromophore composite to develop a practical subcutaneous oxygen sensing platform (Figure 7D–G) [148]. The results showed that β-sheet proteins formed a network through physical crosslink, entrapping and stabilizing PdBMAP. In vivo experiments using three physical states (hyperoxia, normoxia, and hypoxia) proved that the silk/chromophore composite films were suitable for real-time continuous oxygen sensing. This study suggests that silk is an auspicious alternative as a host substrate in implantable and physiological sensing. An aptasensor based on TiO_2 NPs and an SF composite as the probe oligonucleotide platform was fabricated for prostate-specific antigens [201]. The aptasensor had a high selectivity for prostate-specific antigens over bovine serum and lysozyme, and satisfactory reproducibility and stability. The response after it was stored in phosphate buffer for seven days retained 94% of its initial response. The aptasensor detected the prostate-specific antigen in serum real solutions successfully. Moreover, the carbonized silk/AuNPs patch for sweat non-invasive urea detection was fabricated via two steps [204]: First, Au NPs were deposited by heating, during which the tyrosine of silk as a self-reducing agent, and had a conductivity in the range of semiconductivity $(795 \pm 54) \times 10^{-6}$ S/cm. The silk/AuNPs patch was then carbonized. When used as the working electrode of an electrochemical sensor for sweat urea, the carbonized silk/AuNPs patch had a detection range of 0–100 mM with a limit of 20 mM. When used as bioship laser desorption/ionization mass spectrometry (LDI-MS), the silk/AuNPs patch had a detection limit of 8 mM, enabling us to distinguish between normal individuals and kidney prone patients.

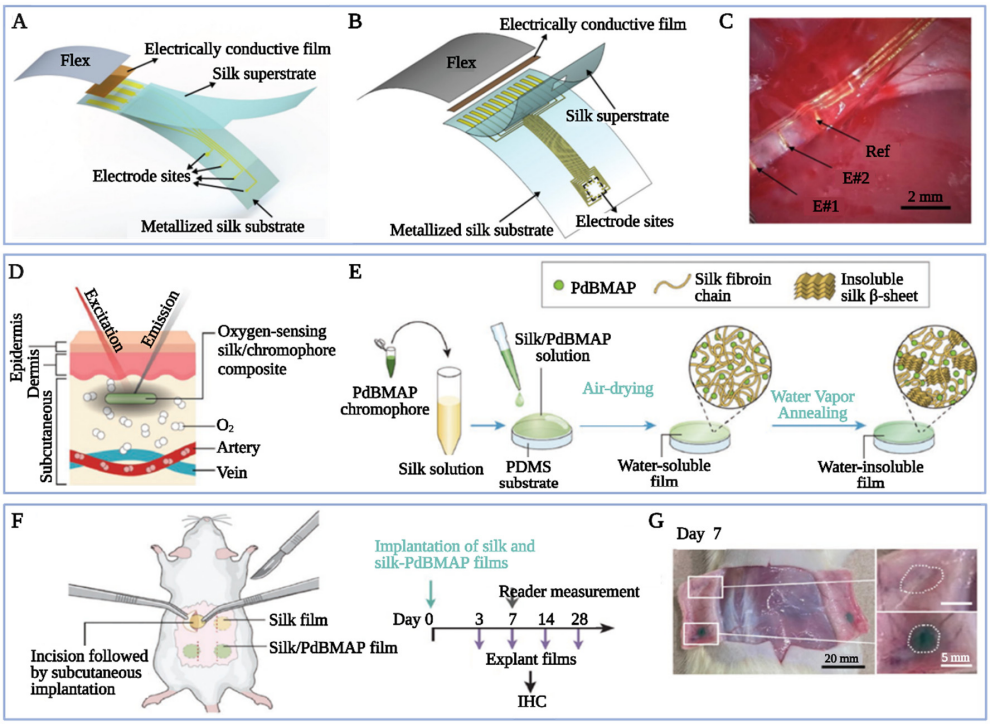

Figure 7. Schematic exploded-view illustration of the construction of a flexible silk electrode array for electroneurograms (**A**) and micro-electrocorticograms (**B**) measurements. (**C**) Photograph of a two-channel silk electrode array deployed as a band-aid on the sciatic nerve of a rat. The diameter is about 600 µm. Adapted with permission from ref. [203]. Copyright 2021, Elsevier. (**D**) Schematic diagram of the continuous oxygen monitoring platform by the phosphorescent silk/chromophore composite film. (**E**) Schematic outlining the silk/chromophore film production. (**F**) Implantation of the silk/chromophore composite film on the back of the animal and its silk/chromophore composite film after 3, 7, 14, and 28 days. (**G**) Integration of the film into the tissue after 7 days. Adapted with permission from ref. [148]. Copyright 2022, Wiley-VCH GmbH.

4.3.2. Silk/Base Metal Composite and Smart Environmental and Health Electronics

In addition to silk/noble metal nanoparticle composites and in vivo micro monitor for biomedicine, silk/metal composites can also be used for physical and chemical detection. Good flexibility enables the material to withdraw various deformations, such as bending, which is vital for creating optoelectronic and biomimetic devices [205]. Silk/metal composites, with excellent flexibility and optical and optoelectronic properties, have been used to develop consumer electronics for food and environment quality monitoring and personal healthcare.

A highly flexible electronic textile sensor was fabricated using the functionalized silk fiber coiled yarns from carbon nanotubes, Ag nanowires, and ionic liquid [EMIM]Tf_2N (Figure 8A–D) [206]. The fabricated textile had an extremely high sensitivity (1.23%/°C) and stability compared with other sensors in temperature sensing [207–209]. Based on the capacitance change of each cross-point of two yarns, the pressure sensing function of the sensor was achieved and very position-dependent, with a sensitivity of 0.136/kPa. Furthermore, a special textile that could sense temperature and pressure with a position precision of 1 mm^2 was fabricated and successfully employed to produce intelligent gloves with capabilities of sensing temperature and weight distributions. In one study, the SF-capped copper NCs (SF/CuNCs) were synthesized using $Cu(NO_3)_2 \cdot 3H_2O$ and SF [187]. The SF/CuNCs exhibited monodispersion and higher sensitivity and selectivity to S^{2-} over various metal ions, anions, and micromolecules. Their practicability as fluorescent nanosensors for detecting S^{2-} was demonstrated in tap and river water samples. SF/CuNCs had a valence between 0 and +1, which confirmed SF served as a protective agent and a reducing agent during synthesis and was consistent with previous studies [188,192]. Like the study in [206], a noble metal Au NP as a functional component and silk as a substrate was used for designing a wireless passive antenna (Figure 8E) [210]. The antenna was conformal and could adhere to curved surfaces tightly. The antenna, with biodegradable and edible components, was demonstrated as a sensor for food quality change by monitoring the ripening process of apples and bananas and the spoilage process of cheese and milk.

Aside from metal ions, silk proteins can also combine with natural nonmetallic materials to form biosensing composites. For instance, silk protein/anthocyanin composites can be used to detect metal ions in aqueous solutions and show the saturation state of metal ion adsorption by the composite [96,211–213]. This is because anthocyanin, a natural water-soluble pigment, exhibits significant color changes upon interaction with metal ions. Owing to the stronger interaction between silk proteins and metal ions compared to anthocyanin, the silk protein component in the composite preferentially combines with metal ions, thereby protecting the anthocyanin [73,90,96,214]. In one study, sericin/anthocyanin nanocomposites were fabricated to enhance the physicochemical stability of anthocyanin [90]. The results showed that the retention ratio of anthocyanin in the composite increased significantly, from 33% to 97.93%, in Cu^{2+} solution after 6 h incubation. Another study showed that the sericin/anthocyanin solution and filter film exhibited a gradual color change from pink to blue in response to varying Zn^{2+} concentrations, with a visually discernable difference at 100 mM Zn^{2+}. For Al^{3+}, the color changed from pink to purple, and the visually noticeable difference occurred at 0.1 mM Al^{3+} (Figure 2B) [96]. These studies manifest that sericin was an appropriate choice for fabricating biosafe and effective metal ion detection instruments, with potential applications in chemical and biological analysis.

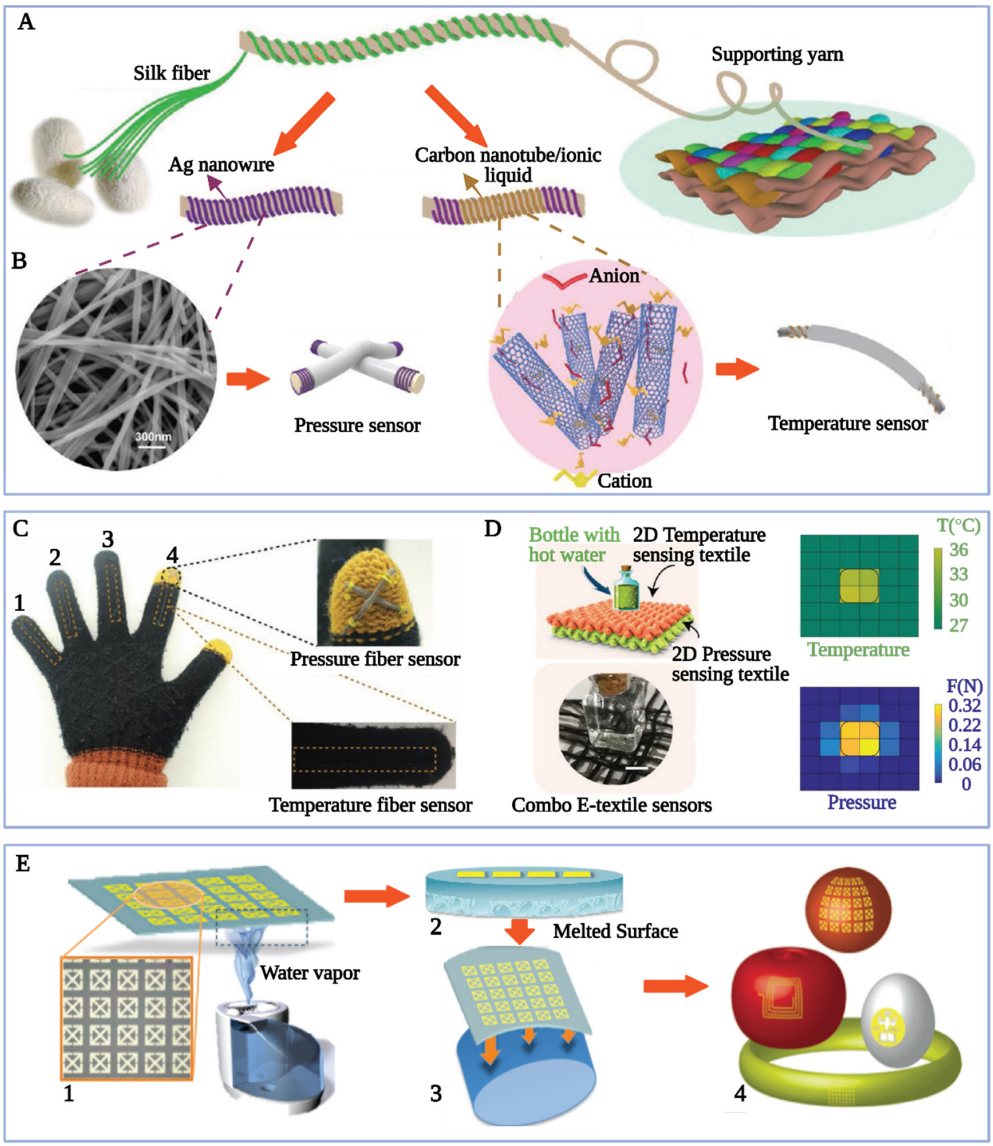

Figure 8. Schematic of the strategy for the fabrication of silk fibers-wrapped combo temperature–pressure sensors: (**A**) Coiling supporting yarns by silkworm silk fibers. (**B**) Coating the silk fiber coiled yarns with temperature or pressure sensing materials (Ag nanowires for pressure sensing, and the mixture of carbon nanotube and an ionic liquid for temperature sensing) and coating the protection or dielectric layers on the functional yarns/fibrous sensors. (**C**) Photographs of the smart gloves with the textile-based pressure and temperature sensors at the ends of four fingers. (**D**) Schematic illustration and image of placing a cup of hot water on the multimode sensing textile (scale bar = 5 mm) and the position-related 3D temperature and pressure sensing: the temperature and pressure distributions of the cup on the combo sensing textile in terms of the relative resistance and capacitance changes, respectively. Adapted with permission from ref. [206]. Copyright 2019, Wiley-VCH GmbH. (**E**) Schematic of steps for rapid transfer of silk antennas onto curved substrates. (1) Water vapor is applied to the back of non-crystalline functionalized silk films, yielding (2) a functionalized film in which the back surface of the film has been partially melted. (3) This melted surface is conformally applied to arbitrary surfaces, yielding (4) applied functional sensors on a variety of surfaces. Adapted with permission from ref. [210]. Copyright 2012, Wiley-VCH GmbH.

4.4. Silk-Based Electrochemical Materials

Aside from biosensing use, silk/metal composites show an increasing application in electrochemistry, especially in electrocatalysis and energy storage for power supply, owing to the strong binding between silk proteins and metals and the outstanding properties of silk materials mainly including good flexibility, degradability, and biocompatibility that

imparts silk/metal composites with the properties of conductive materials and various application forms [154,215].

4.4.1. Energy-Storage Materials for Power Supply

The interaction of silk proteins with metal ions endows them with excellent electrochemical and electroconductive properties. Accordingly, they are used to make micro energy-storing devices to supply power to implantable devices, wearable smart electronics, etc. [216–218].

In silk-based energy storage devices, the degradable micro battery has captured the most attention of researchers. As natural proteins with exceptional processibility, silk proteins in these micro batteries are used as substrates, encapsulation coatings, insulating spacers, or functional components of all-solid-state electrolytes and electrodes [219–222]. Specifically, a sandwich-structured garnet $Li_7La_3Zr_2O_{12}$ (LLZO) ceramic fabric composite solid electrolyte (LLZO CF-CSE) was fabricated by using silk as a template (Figure 9A) [223]. The LLZO CF-CSE exhibited remarkable electrochemical stability (wide electrochemical short window of 5.1 V vs. Li^+/Li) and thermostability. The lithium metal battery prepared using LLZO CF-CSE could stably run with a short circuit for 700 h at 50 °C. The all-solid-state lithium battery Li | LLZO CF-CSE | $LiFePO_4$ had high reversible capacity and excellent cycle stability. Its specific capacity was 149.3 mAh/g after 100 cycles at 0.2 °C, and 107.2 mAh/g after 500 cycles at 0.1 °C. Furthermore, silk proteins have been a popular component for transient implantable energy devices [55,217]. For instance, a biodegradable ion-conducting membrane was designed by immobilizing a biocompatible ionic liquid (choline nitrate, [Ch][NO_3]) in silk (Figure 9B,C) [55]. By using this membrane as an electrolyte, a biodegradable thin-film Mg battery was fabricated, which used Au-SF as its cathode and AZ31-SF as its anode, and was encapsulated by silk. Results showed that the designed polymer electrolyte [SF-[Ch][NO_3]] (1:3)] had an ionic conductivity of 3.4 Sm/cm and a two-day degradation profile. The encapsulated thin-film battery had a capacity of 0.06 mAh/cm^2 at a current density of 10 μA/cm^2 and a degradation profile of 45 days. Additionally, the dendrite formation precludes the reversible cycle in lithium-ion metal batteries [224,225]. However, a Ni/silk/Li anode, fabricated using a flexible Ni/silk fiber and Li metals, could reduce the wanton formation of lithium dendrites by inducing uniform Li deposition (Figure 9D) [226]. The flexible Ni/silk fiber was prepared using the catalyzer Ni particles to graphitize silk fibers. The results showed that the Ni/silk/Li anode exhibited better electrochemical performances than the silk-Li anode. It had a longer lifespan of 800 h, an overpotential of 23.5 mV, and a high coulombic efficiency of 98.35% for the half cells. These properties manifested that the Ni/silk/Li anode enabled the mitigation of dendrite formation. The prevention of lithium dendrites by silk-based materials also has been demonstrated in other studies [227–230].

In addition to micro batteries, the silk proteins also have been applied in flexible supercapacitors [231–234]. In a study, silk textile is directly carbonized to make a conductive free-standing substrate for preparing low-cost, flexible, tough, and up-scalable supercapacitor electrodes [216]. The results showed that the prepared electrode's areal capacitance was 362 mF/cm^2, clearly greater than that of the MXene-based flexible electrodes. The cyclic voltammogram (CV) test with up to 10,000 cycles demonstrated the prepared electrodes also had outstanding stability. The CV curves of the supercapacitor made from carbonized silk cloth and $Ti_3C_2T_x$ changed a little under bending at 120°, indicating the $Ti_3C_2T_x$ was tightly coated on carbonized silk cloth. Likewise, a hydrogen electrode was created by stimulating the collagen fiber network and proteoglycan in cartilage using a silk nanofiber network and polyvinyl alcohol [235]. The supercapacitor had the highest capacitance (13.62 F/cm^2) among the currently reported polyvinyl alcohol capacitors and an energy density of 1.2098 mWh/cm^2, owing to the effective connection between the silk nanofiber network and carbon nanotubes. Overall, using silk-based materials imparts higher capacitance and resilience to capacitors.

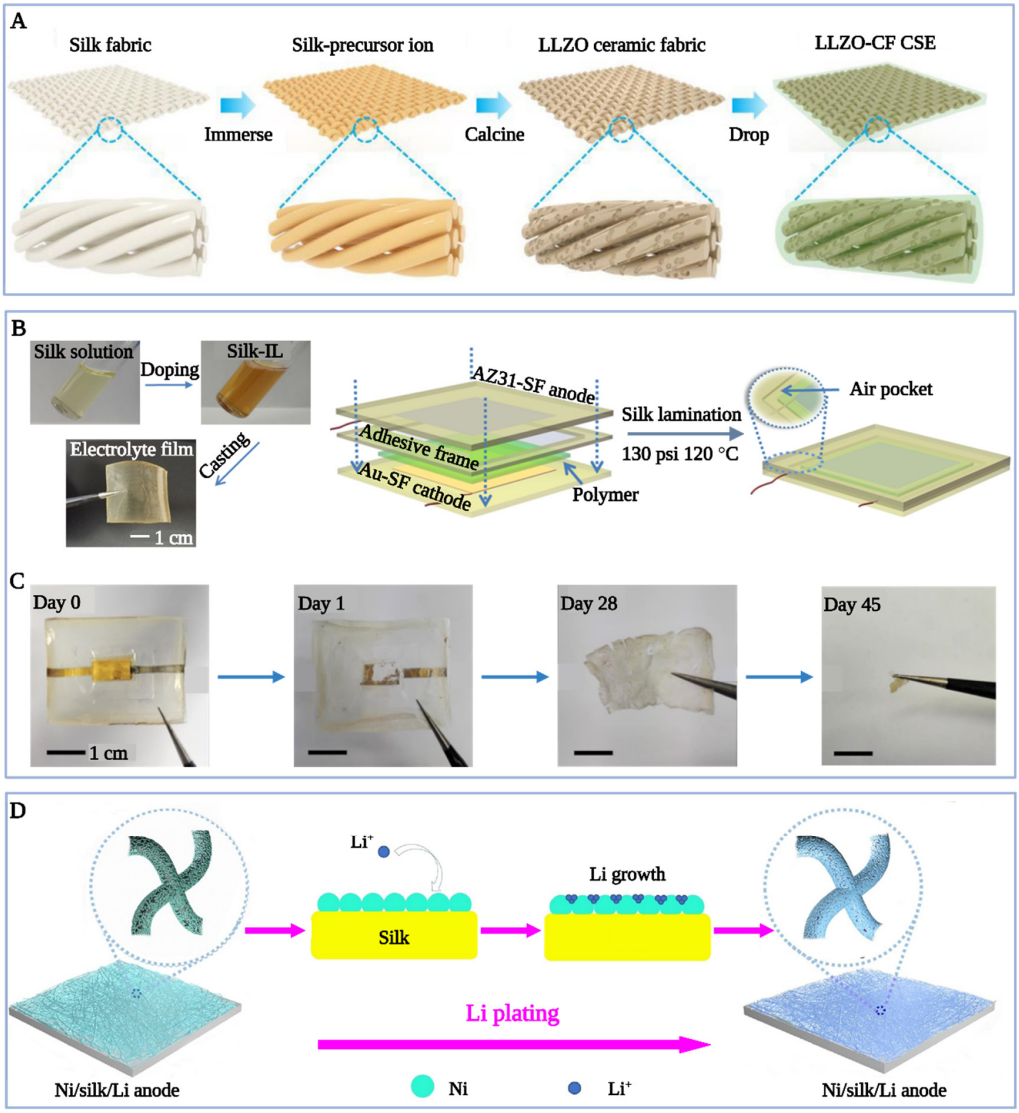

Figure 9. (**A**) Schematic of the preparation of the $Li_7La_3Zr_2O_{12}$ ceramic fabric composite solid electrolyte (LLZOCF–CSE). Adapted with permission from ref. [223]. Copyright 2022, Elsevier. (**B**) Fabrication procedures and a digital image of a polymer electrolyte film (SF:[Ch][NO_3], weight ratio of 1:3) and schematic of an encapsulated battery with a silk pocket. (**C**) Optical images demonstrating the biodegradation profile of an encapsulated battery (device size of 3.6 × 2.7 × 0.017 cm^3) in buffered protease solution at 37 °C. Adapted with permission from ref. [55]. Copyright 2017, American Chemical Society. (**D**) Scheme of Li plating process on the Ni/silk/Lithium anode. Adapted with permission from ref. [226]. Copyright 2023, Wiley-VCH GmbH.

4.4.2. Carbon-Based Electrocatalytic Composites

Silk/metal composites with catalytic activity also have been studied [236,237]. The advantages of SF for constructing catalytic components are attributed to its elemental composition and molecular structure [238]. First, the SF molecule is rich in C, O, N, and S atoms; accordingly, they can act as precursors for fabricating heteroatom-doped carbon, especially N-doped carbon. Second, the SF's amino acids have special spatial effects and strong chelation with metal ions, which are beneficial to the formation of enhanced active sites, smaller particle sizes, and an enhanced dispersity of active particles. Therefore, SF molecules are superior catalyst carriers. Third, the SF's structures facilitate the fabrication of porous carbon nanomaterials, which have better geometry, high surface area, and heat transfer properties, and then enhance the heat and electron transfers in catalysis. Rapid and environmentally friendly synthesis of flower-like gold nanoparticles/reduced

graphene oxide (Au NPs/RGO) composites was achieved using regenerated silk fibroin (RSF) (Figure 10A) [239]. RSF was obtained by breaking the hydrogen bonds in SF and dissolving it in water. RSF could be easily and tightly absorbed onto the RGO surface owing to the formation of hydrogen bonds and π-π stacking between them. Meanwhile, it could absorb metal NPs because -COOH and -NH_2 groups provided binding sites for nucleation. In other words. RSF served as an adhesive, connecting RGO and Au NPs to form flowerlike Au NPs/RGO. The electrochemical experiment showed that the flower-like Au NPs/RGO composites exhibited better catalytic performance for ORR than branched Au NPs/RGO composites and spherical Au (I, II) NPs/RGO composites [239]. In contrast to using noble metals, novel nitrogen (N) and trace iron (Fe) co-doped 3D porous carbon (NFe_x-C) was synthesized as an excellent ORR catalyst from a salt-induced silk gel (Figure 10B) [240]. The salt-induced silk gel spontaneously improved the porosity and boosted the ORR activity. The cyclic voltammetry and linear sweep voltammetry tests showed that NFe_x-C had a remarkably higher positive initial potential (0.274 V vs. Ag/AgCl) and half-wave potential ($E_{1/2}$) (0.095 V vs. Ag/AgCl) than commercial Pt/C catalysts. In the same year, 2D porous carbon nanosheets with atomically-dispersed Fe–N_x–C active sites and very large specific surface areas (about 2105 m^2/g) were created through dissolving RSF in $FeCl_3$ and $ZnCl_2$ aqueous solution and thermal treatment (Figure 10C) [241]. The obtained silk-driven carbon nanosheets demonstrated excellent electrochemical properties to ORR with a half-potential of 0.853 V and outstanding stability with just 11 mV loss in $E_{1/2}$ after 30,000 cycles, and also good catalytic activity to OER. By contrast, nanoscale nickel-cobalt-iron (NiCoFe) alloys were anchored in boron (B) and nitrogen (N) co-doped SF carbon aerogel to synthesize a specialized OER electrocatalyst [242]. The optimized electrocatalyst (BN/CA-NiCoFe-600) possessed low overpotential (321 mV at a current density of 10 mA/cm^2), low Tafel slope (42 mV/dec), and superior stability and durability. The electron and heat transfer were improved by the SF aerogel. Other SF-derived carbon aerogels anchored with metal ions have been created as electrocatalysts for OER [57], HER [57,236,243], and CO_2-to-CO conversion [244]. The above research demonstrates the applicability of silk proteins as precursors to design efficient and cost-effective electrochemical catalysts.

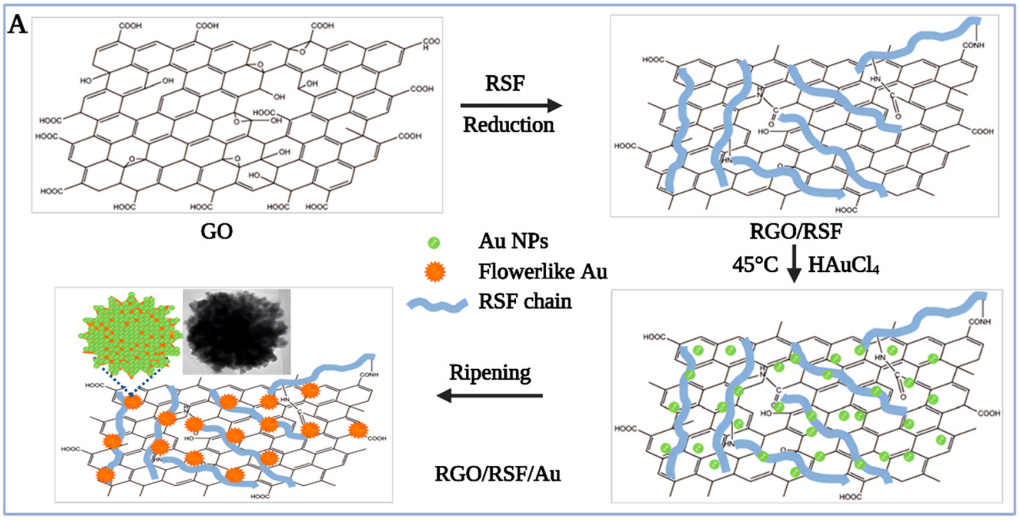

Figure 10. *Cont.*

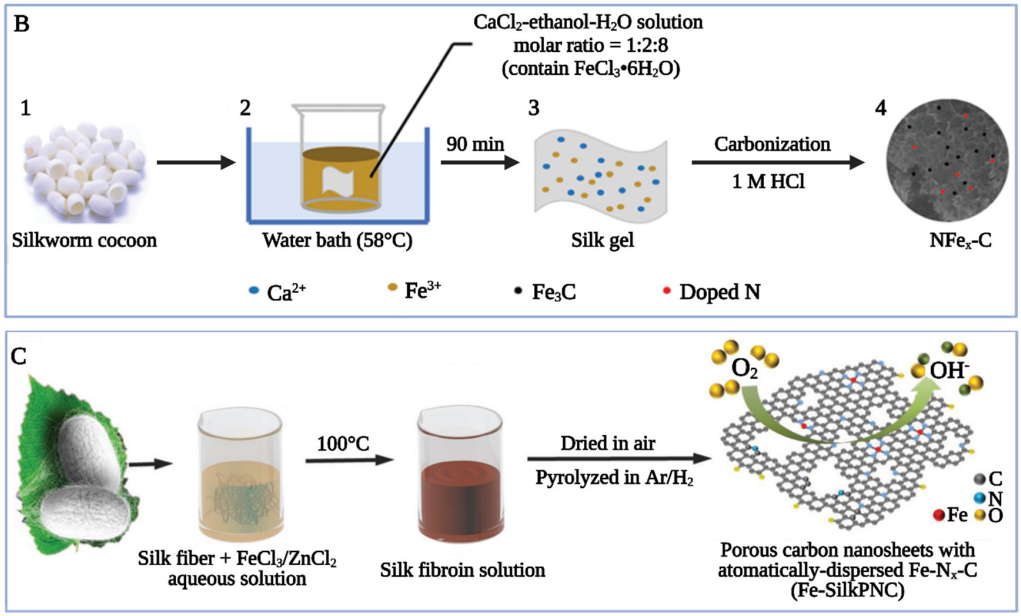

Figure 10. (**A**) Schematic diagram of the procedure for the synthesis of flower-like Au/RGO composite. Adapted with permission from ref. [239]. Copyright 2013, American Chemical Society. (**B**) The synthetic route of NFe_X-C from a salt-induced silk gel: (1) silkworm cocoons, (2) the silkworm cocoon incubated in a water bath (58 °C), (3) the salt-induced silk gel precursor of NFe_X-C, and (4) the achieved NFe_X-C catalysts. Adapted with permission from ref. [240]. Copyright 2019, The Royal Society of Chemistry. (**C**) Schematic illustration of the preparation process for porous carbon nanosheets with automatically-dispersed Fe-N_x-C (Fe-SilkPNC). Adapted with permission from ref. [241]. Copyright 2019, Wiley-VCH GmbH.

5. Conclusions

As one of the most popular natural fibers, silk produced by the *Bombyx mori* L. silkworm, silk's applications have been extended from traditional textiles to the environmental protection field and advanced biomaterials. Silk is composed of SF and sericin. These two silk proteins process many polar functional groups including carboxyl, hydroxyl, amino group, and amide group, enabling strong adsorption of silk proteins to metal ions. Based on this adsorption, plus the outstanding properties including biocompatibility, biodegradability, and processability, silk's performance can not only be modified but also can be used to protect the environment and can be combined with metal nanostructures to prepare advanced biomaterials. Regarding performance optimization, silk's mechanical performance, flame retardancy, and color fastness can be enhanced through binding with some metal ions, making silk meet today's new expectations for textiles. For environmental protection, SF and sericin can be used alone or combined with other natural or synthetic polymers to fabricate environmentally sound and efficient adsorbent materials generally in the form of film and particle. Concerning advanced biomaterial, silk proteins can be combined with metal ions to form biosensing materials and electrocatalytic materials, and during most of the combinations, the metal ions are reduced to zero-value metal atoms. In biosensing materials, the silk/noble metal nanostructure composites can be used to produce in vivo micro materials due to their biocompatibility, while silk/base metal composites are promising for smart environmental and health consumer electronics. The electrochemical materials include energy-storage materials to supply power to implantable devices and carbon-based electrocatalytic composites. The review indicates that these novel applications of silk proteins, based on their interactions with metal ions, shed light on further study of the property modification and the potential use in other fields of silk proteins and similar natural polymers.

Author Contributions: Conceptualization—T.Z., P.C. and L.Z. Writing—Q.W. and L.Z. Writing—review and editing—Y.C., Y.S. and J.Y. Supervision—T.Z. and P.C. Project administration—T.Z. and P.C. All authors have read and agreed to the published version of the manuscript.

Funding: This research was funded by the National Natural Science Foundation of China, grant number 22278395.

Institutional Review Board Statement: Not applicable.

Informed Consent Statement: Not applicable.

Data Availability Statement: Not applicable.

Conflicts of Interest: Author Yi Su was employed by the company Zhejiang Ecogreen Ecological Technology Co., Ltd. The remaining authors declare that the research was conducted in the absence of any commercial or financial relationships that could be construed as a potential conflict of interest.

Abbreviations

Au NPs/RGO	gold nanoparticles/reduced graphene oxide
BET	Brunauer–Emmett–Teller
BN/CA-NiCoFe-600	boron (B), nitrogen (N) co-doped SF carbon aerogel that was anchored with nickel-cobalt-iron (NiCoFe) alloys
CA	cellulose acetate
CPP	casein phosphopeptide
$CuCoFe_2O_4$	SF, cellulose, and β-cyclodextrin-based hydrogel modified by magnetic copper-doped cobalt ferrite
EDTA	ethylenediaminetetraacetic acid
EDX	energy dispersive X-ray spectroscopy
$E_{1/2}$	half-wave potential
FE-SEM	field emission scanning electron microscopy
Fe-SilkPNC	porous carbon nanosheets with automatically-dispersed Fe-N_x-C
HER	hydrogen evolution reaction
H-chain	heavy chain
LDI-MS	laser desorption/ionization mass spectrometry
LLZO CF–CSE	$Li_7La_3Zr_2O_{12}$ ceramic fabric composite solid electrolyte
LM/NaAlg	liquid metal alginate-coated NPs
LOI	limiting oxygen index
L-chain	light chain
MTT	3-(4,5)-dimethylthiahiazo (-z-y1)-3,5-di- phenytetrazoliumromide
NC(s)	nanocluster(s)
NFe_x-C	nitrogen (N) and trace iron (Fe) co-doped 3D porous carbon
NP(s)	nanoparticle(s)
OER	oxygen evolution reaction
ORR	oxygen reduction reaction
PAA	poly-acrylic acid
PBS	phosphate-buffered saline
PDL(s)	poly dentate ligands
PdBMAP	Pd^{2+} tetramethacrylated benzoporphyrin
PEEK	polyetheretherketone
RGO	reduced graphene oxide
RSF	regenerated silk fibroin
S	sericin
SC	sericin/anthocyanin
SF	silk fibroin
STEM	scanning transmission electron microscopy
TEM	transmission electron microscope
UV (A)	ultraviolet (A)
UV-Vis	ultraviolet and visible

WK	wool keratose
2D	two-dimensional
3D	three-dimensional

References

1. Vainker, S.J. *Chinese Silk: A Cultural History*; Rutgers University Press: New Brunswick, NJ, USA, 2004.
2. Slonimskiy, Y.B.; Egorkin, N.A.; Ashikhmin, A.A.; Friedrich, T.; Maksimov, E.G.; Sluchanko, N.N. Reconstitution of the functional Carotenoid-Binding Protein from silkworm in *E. coli*. *Int. J. Biol. Macromol.* **2022**, *214*, 664–671. [CrossRef] [PubMed]
3. Dusi, G.G.; Marques, G.S.; Kienteca, M.L.; Gimenes, M.L.; Cerutti, M.L.M.N.; da Silva, V.R. Biosorption investigation of Cu(II) ions from aqueous solutions using sericin–alginate particles: Kinetic, equilibrium, and thermodynamic. *Sustain. Chem. Pharm.* **2022**, *25*, 100601. [CrossRef]
4. Chen, K.; Li, Y.H.; Li, Y.B.; Pan, W.S.; Tan, G.X. Silk Fibroin Combined with Electrospinning as a Promising Strategy for Tissue Regeneration. *Macromol. Biosci.* **2023**, *23*, 2200380. [CrossRef] [PubMed]
5. Chen, S.; Matsumoto, H.; Moro-oka, Y.; Tanaka, M.; Miyahara, Y.; Suganami, T.; Matsumoto, A. Smart Microneedle Fabricated with Silk Fibroin Combined Semi-interpenetrating Network Hydrogel for Glucose-Responsive Insulin Delivery. *ACS Biomater. Sci. Eng.* **2019**, *5*, 5781–5789. [CrossRef] [PubMed]
6. Cheng, T.-H.; Yang, Z.-Y.; Tang, R.-C.; Zhai, A.-D. Functionalization of silk by silver nanoparticles synthesized using the aqueous extract from tea stem waste. *J. Mater. Res. Technol.* **2020**, *9*, 4538–4549. [CrossRef]
7. Li, G.; Li, Y.; Chen, G.; He, J.; Han, Y.; Wang, X.; Kaplan, D.L. Silk-Based Biomaterials in Biomedical Textiles and Fiber-Based Implants. *Adv. Healthc. Mater.* **2015**, *4*, 1134–1151. [CrossRef] [PubMed]
8. Guo, Z.; Xie, W.; Gao, Q.; Wang, D.; Gao, F.; Li, S.; Zhao, L. In situ biomineralization by silkworm feeding with ion precursors for the improved mechanical properties of silk fiber. *Int. J. Biol. Macromol.* **2018**, *109*, 21–26. [CrossRef] [PubMed]
9. He, H.; Cai, R.; Wang, Y.; Tao, G.; Guo, P.; Zuo, H.; Chen, L.; Liu, X.; Zhao, P.; Xia, Q. Preparation and characterization of silk sericin/PVA blend film with silver nanoparticles for potential antimicrobial application. *Int. J. Biol. Macromol.* **2017**, *104*, 457–464. [CrossRef]
10. Liu, M.; Min, L.; Zhu, C.; Rao, Z.; Liu, L.; Xu, W.; Luo, P.; Fan, L. Preparation, characterization and antioxidant activity of silk peptides grafted carboxymethyl chitosan. *Int. J. Biol. Macromol.* **2017**, *104*, 732–738. [CrossRef]
11. Liu, Q.; Wang, X.; Tan, X.; Xie, X.; Dong, H.; Li, X.; Li, Y.; Zhao, P.; Xia, Q. Disruption of the Metal Ion Environment by EDTA for Silk Formation Affects the Mechanical Properties of Silkworm Silk. *Int. J. Mol. Sci.* **2019**, *20*, 3026. [CrossRef]
12. Chen, J.; Venkatesan, H.; Hu, J. Chemically Modified Silk Proteins. *Adv. Eng. Mater.* **2018**, *20*, 1700961. [CrossRef]
13. Sun, J.; Su, J.; Ma, C.; Göstl, R.; Herrmann, A.; Liu, K.; Zhang, H. Fabrication and Mechanical Properties of Engineered Protein-Based Adhesives and Fibers. *Adv. Mater.* **2020**, *32*, 1906360. [CrossRef] [PubMed]
14. Guo, C.; Zhang, J.; Jordan, J.S.; Wang, X.; Henning, R.W.; Yarger, J.L. Structural Comparison of Various Silkworm Silks: An Insight into the Structure–Property Relationship. *Biomacromolecules* **2018**, *19*, 906–917. [CrossRef] [PubMed]
15. Teramoto, H.; Kojima, K.; Iga, M.; Yoshioka, T. Unique Material Properties of Bombyx mori Silk Fiber Incorporated with 3-Azidotyrosine. *Biomacromolecules* **2023**, *24*, 4208–4217. [CrossRef]
16. Wang, X.; Zhao, P.; Li, Y.; Yi, Q.; Ma, S.; Xie, K.; Chen, H.; Xia, Q. Modifying the mechanical properties of silk fiber by genetically disrupting the ionic environment for silk formation. *Biomacromolecules* **2015**, *16*, 3119–3125. [CrossRef] [PubMed]
17. Liu, Q.; Wang, X.; Tan, X.; Xie, X.; Li, Y.; Zhao, P.; Xia, Q. A strategy for improving the mechanical properties of silk fiber by directly injection of ferric ions into silkworm. *Mater. Des.* **2018**, *146*, 134–141. [CrossRef]
18. Wu, Y.X.; Huang, Y.T.; Guan, J.P.; Cheng, X.W.; Xu, J.T.; Chen, G.Q. Facile preparation of effective flame retardant silk fabric by the metal salt adsorption approach. *Polym. Degrad. Stab.* **2020**, *182*, 109378. [CrossRef]
19. Zhou, Y.; Tang, R.-C.; Xing, T.; Guan, J.-P.; Shen, Z.-H.; Zhai, A.-D. Flavonoids-metal salts combination: A facile and efficient route for enhancing the flame retardancy of silk. *Ind. Crops Prod.* **2019**, *130*, 580–591. [CrossRef]
20. Malucelli, G.; Bosco, F.; Alongi, J.; Carosio, F.; Di Blasio, A.; Mollea, C.; Cuttica, F.; Casale, A. Biomacromolecules as novel green flame retardant systems for textiles: An overview. *RSC Adv.* **2014**, *4*, 46024–46039. [CrossRef]
21. Tang, B.; Poma, G.; Bastiaensen, M.; Yin, S.-S.; Luo, X.-J.; Mai, B.-X.; Covaci, A. Bioconcentration and biotransformation of organophosphorus flame retardants (PFRs) in common carp (*Cyprinus carpio*). *Environ. Int.* **2019**, *126*, 512–522. [CrossRef]
22. Vorkamp, K.; Balmer, J.; Hung, H.; Letcher, R.J.; Rigét, F.F.; de Wit, C.A. Current-use halogenated and organophosphorous flame retardants: A review of their presence in Arctic ecosystems. *Emerg. Contam.* **2019**, *5*, 179–200. [CrossRef]
23. Mohsin, M.; Ahmad, S.W.; Khatri, A.; Zahid, B. Performance enhancement of fire retardant finish with environment friendly bio cross-linker for cotton. *J. Clean. Prod.* **2013**, *51*, 191–195. [CrossRef]
24. Song, P.; Fang, Z.; Tong, L.; Jin, Y.; Lu, F. Effects of metal chelates on a novel oligomeric intumescent flame retardant system for polypropylene. *J. Anal. Appl. Pyrolysis* **2008**, *82*, 286–291. [CrossRef]
25. Zhang, W.; Yang, Z.Y.; Tang, R.C.; Guan, J.P.; Qiao, Y.F. Application of tannic acid and ferrous ion complex as eco-friendly flame retardant and antibacterial agents for silk. *J. Clean. Prod.* **2020**, *250*, 119545. [CrossRef]
26. Teli, M.; Paul, R. Novel natural dye from coffee seed coat. *Int. Dyer* **2006**, *191*, 29–32.
27. Tehrani, M.; Ghaheh, F.S.; Beni, Z.T.; Rahimi, M. Extracted dyes' stability as obtained from spent coffee grounds on silk fabrics using eco-friendly mordants. *Environ. Sci. Pollut. Res.* **2023**, *30*, 68625–68635. [CrossRef] [PubMed]

28. Yin, Y.; Fei, L.; Wang, C. Optimization of natural dye extracted from phytolaccaceae berries and its mordant dyeing properties on natural silk fabric. *J. Nat. Fibers* **2018**, *15*, 69–79. [CrossRef]
29. Bhavsar, P.; Dalla Fontana, G.; Tonin, C.; Patrucco, A.; Zoccola, M. Superheated water hydrolyses of waste silkworm pupae protein hydrolysate: A novel application for natural dyeing of silk fabric. *Dyes Pigm.* **2020**, *183*, 108678. [CrossRef]
30. Gupta, S.; Nighojkar, A.; Mayilswamy, N.; Kandasubramanian, B. Recent Trends in the Application of Silk-Based Composites for Remediation of Toxic Contaminants from Wastewater. *J. Polym. Environ.* **2022**, *31*, 2243–2272. [CrossRef]
31. Chen, B.; Ma, Q.; Tan, C.; Lim, T.T.; Huang, L.; Zhang, H. Carbon-based sorbents with three-dimensional architectures for water remediation. *Small* **2015**, *11*, 3319–3336. [CrossRef]
32. Jain, M.; Yadav, M.; Kohout, T.; Lahtinen, M.; Garg, V.K.; Sillanpää, M. Development of iron oxide/activated carbon nanoparticle composite for the removal of Cr(VI), Cu(II) and Cd(II) ions from aqueous solution. *Water Resour. Ind.* **2018**, *20*, 54–74. [CrossRef]
33. Aydin, D. A novel turn on fluorescent probe for the determination of Al^{3+} and Zn^{2+} ions and its cells applications. *Talanta* **2020**, *210*, 120615. [CrossRef] [PubMed]
34. Zhou, W.; He, J.; Cui, S.; Gao, W. Preparation of electrospun silk fibroin/Cellulose Acetate blend nanofibers and their applications to heavy metal ions adsorption. *Fibers Polym.* **2011**, *12*, 431–437. [CrossRef]
35. Li, N.; Zhang, L.; Chen, Y.; Fang, M.; Zhang, J.; Wang, H. Highly Efficient, Irreversible and Selective Ion Exchange Property of Layered Titanate Nanostructures. *Adv. Funct. Mater.* **2012**, *22*, 835–841. [CrossRef]
36. Singh, S.P.; Rathinam, K.; Kasher, R.; Arnusch, C.J. Hexavalent chromium ion and methyl orange dye uptake via a silk protein sericin–chitosan conjugate. *RSC Adv.* **2018**, *8*, 27027–27036. [CrossRef] [PubMed]
37. Wang, S.; Ning, H.; Hu, N.; Huang, K.; Weng, S.; Wu, X.; Wu, L.; Liu, J.; Alamusi. Preparation and characterization of graphene oxide/silk fibroin hybrid aerogel for dye and heavy metal adsorption. *Compos. Part B Eng.* **2019**, *163*, 716–722. [CrossRef]
38. Zhang, Y.; Peng, S.; Li, X.; Wang, X.; Jiang, J.; Liu, X.; Wang, L. Design and function of lignin/silk fibroin-based multilayer water purification membranes for dye adsorption. *Int. J. Biol. Macromol.* **2023**, *253*, 126863. [CrossRef] [PubMed]
39. Babu Busi, K.; Palanivel, M.; Kanta Ghosh, K.; Basu Ball, W.; Gulyás, B.; Padmanabhan, P.; Chakrabortty, S. The Multifarious Applications of Copper Nanoclusters in Biosensing and Bioimaging and Their Translational Role in Early Disease Detection. *Nanomaterials* **2022**, *12*, 301. [CrossRef]
40. Yang, X.; Sun, J.-K.; Kitta, M.; Pang, H.; Xu, Q. Encapsulating highly catalytically active metal nanoclusters inside porous organic cages. *Nat. Catal.* **2018**, *1*, 214–220. [CrossRef]
41. Xiao, Y.; Wu, Z.; Yao, Q.; Xie, J. Luminescent metal nanoclusters: Biosensing strategies and bioimaging applications. *Aggregate* **2021**, *2*, 114–132. [CrossRef]
42. Zhao, R.; Xiang, J.; Wang, B.; Chen, L.; Tan, S. Recent Advances in the Development of Noble Metal NPs for Cancer Therapy. *Bioinorg. Chem. Appl.* **2022**, *2022*, 2444516. [CrossRef] [PubMed]
43. Chen, J.; Liu, Y.; Xiong, Y.; Wei, D.; Peng, J.; Mahmud, S.; Liu, H. Konjac glucomannan reduced-stabilized silver nanoparticles for mono-azo and di-azo contained wastewater treatment. *Inorganica Chim. Acta* **2021**, *515*, 120058. [CrossRef]
44. Restrepo, C.V.; Villa, C.C. Synthesis of silver nanoparticles, influence of capping agents, and dependence on size and shape: A review. *Environ. Nanotechnol. Monit. Manag.* **2021**, *15*, 100428. [CrossRef]
45. Nguyen, N.T.-P.; Nguyen, L.V.-H.; Thanh, N.T.; Toi, V.V.; Ngoc Quyen, T.; Tran, P.A.; David Wang, H.-M.; Nguyen, T.-H. Stabilization of silver nanoparticles in chitosan and gelatin hydrogel and its applications. *Mater. Lett.* **2019**, *248*, 241–245. [CrossRef]
46. Dong, Q.; Su, H.L.; Zhang, D. In situ depositing silver nanoclusters on silk fibroin fibers supports by a novel biotemplate redox technique at room temperature. *J. Phys. Chem. B* **2005**, *109*, 17429–17434. [CrossRef] [PubMed]
47. Wang, X.M.; Gao, W.R.; Xu, S.P.; Xu, W.Q. Luminescent fibers: In situ synthesis of silver nanoclusters on silk via ultraviolet light-induced reduction and their antibacterial activity. *Chem. Eng. J.* **2012**, *210*, 585–589. [CrossRef]
48. Wang, Z.; Li, J.; Shao, C.; Lin, X.; Yang, Y.; Chen, N.; Wang, Y.; Qu, L. Moisture power in natural polymeric silk fibroin flexible membrane triggers efficient antibacterial activity of silver nanoparticles. *Nano Energy* **2021**, *90*, 106529. [CrossRef]
49. Ru, M.; Hai, A.M.; Wang, L.; Yan, S.; Zhang, Q. Recent progress in silk-based biosensors. *Int. J. Biol. Macromol.* **2023**, *224*, 422–436. [CrossRef]
50. Lv, L.; Wu, X.; Yang, Y.; Hang, X.; Mezzenga, R.; Li, C. Trans-Scale 2D Synthesis of Millimeter-Large Au Single Crystals via Silk Fibroin Templates. *ACS Sustain. Chem. Eng.* **2018**, *6*, 12419–12425. [CrossRef]
51. Choi, J.H.; Choi, M.; Kang, T.; Ho, T.S.; Choi, S.H.; Byun, K.M. Combination of Porous Silk Fibroin Substrate and Gold Nanocracks as a Novel SERS Platform for a High-Sensitivity Biosensor. *Biosensors* **2021**, *11*, 441. [CrossRef]
52. Xu, Z.; Shi, L.; Yang, M.; Zhu, L. Preparation and biomedical applications of silk fibroin-nanoparticles composites with enhanced properties—A review. *Mater. Sci. Eng. C* **2019**, *95*, 302–311. [CrossRef]
53. Zhang, G.; Geng, F.; Zhao, T.; Zhou, F.; Zhang, N.; Zhang, S.; Deng, C. Biocompatible symmetric Na-ion microbatteries with sphere-in-network heteronanomat electrodes realizing high reliability and high energy density for implantable bioelectronics. *ACS Appl. Mater. Interfaces* **2018**, *10*, 42268–42278. [CrossRef] [PubMed]
54. He, H.-Z.; Zhang, Y.; Li, Y.; Wang, P. Recent innovations of silk-derived electrocatalysts for hydrogen evolution reaction, oxygen evolution reaction and oxygen reduction reaction. *Int. J. Hydrog. Energy* **2021**, *46*, 7848–7865. [CrossRef]
55. Jia, X.; Wang, C.; Ranganathan, V.; Napier, B.; Yu, C.; Chao, Y.; Forsyth, M.; Omenetto, F.G.; MacFarlane, D.R.; Wallace, G.G. A Biodegradable Thin-Film Magnesium Primary Battery Using Silk Fibroin–Ionic Liquid Polymer Electrolyte. *ACS Energy Lett.* **2017**, *2*, 831–836. [CrossRef]

56. Zheng, S.-M.; Yuan, Z.-H.; Dionysiou, D.D.; Zhong, L.-B.; Zhao, F.; Yang, J.-C.E.; Zheng, Y.-M. Silkworm cocoon waste-derived nitrogen-doped hierarchical porous carbon as robust electrode materials for efficient capacitive desalination. *Chem. Eng. J.* **2023**, *458*, 141471. [CrossRef]
57. He, H.; Zhang, Y.; Zhang, W.; Li, Y.; Wang, Y.; Wang, P.; Hu, D. Dual Metal-Loaded Porous Carbon Materials Derived from Silk Fibroin as Bifunctional Electrocatalysts for Hydrogen Evolution Reaction and Oxygen Evolution Reaction. *ACS Appl. Mater. Interfaces* **2021**, *13*, 30678–30692. [CrossRef] [PubMed]
58. Liu, J.; Wei, L.; Wang, H.; Lan, G.; Yang, H.; Shen, J. Silk gel-based N self-doped porous activated carbon as an efficient electrocatalyst in neutral, alkaline and acidic medium. *Fuel* **2021**, *287*, 119485. [CrossRef]
59. Xi, R.; Li, Y.; Zhang, Y.; Wang, P.; Hu, D. Effects of activation method on biomass carbon-based materials used for electrochemical hydrogen evolution reaction catalyst. *Int. J. Hydrog. Energy* **2023**, *in press*. [CrossRef]
60. Padamwar, M.N.; Pawar, A.P.; Daithankar, A.V.; Mahadik, K.R. Silk sericin as a moisturizer: An in vivo study. *J. Cosmet. Dermatol.* **2005**, *4*, 250–257. [CrossRef]
61. Tomeh, M.A.; Hadianamrei, R.; Zhao, X. Silk Fibroin as a Functional Biomaterial for Drug and Gene Delivery. *Pharmaceutics* **2019**, *11*, 494. [CrossRef]
62. Inoue, S.; Tanaka, K.; Arisaka, F.; Kimura, S.; Ohtomo, K.; Mizuno, S. Silk fibroin of Bombyx mori is secreted, assembling a high molecular mass elementary unit consisting of H-chain, L-chain, and P25, with a 6:6:1 molar ratio. *J. Biol. Chem.* **2000**, *275*, 40517–40528. [CrossRef]
63. Tanaka, K.; Inoue, S.; Mizuno, S. Hydrophobic interaction of P25, containing Asn-linked oligosaccharide chains, with the H-L complex of silk fibroin produced by Bombyx mori. *Insect Biochem. Mol. Biol.* **1999**, *29*, 269–276. [CrossRef] [PubMed]
64. Rastogi, S.; Kandasubramanian, B. Progressive trends in heavy metal ions and dyes adsorption using silk fibroin composites. *Environ. Sci. Pollut. Res.* **2020**, *27*, 210–237. [CrossRef] [PubMed]
65. Hao, Z.; Long, D.; Zhang, Y.; Umuhoza, D.; Dai, J.; Xu, Z.; Zhang, G.; Meng, W.; Xiang, Z.; Zhao, A. New insight into the mechanism of in vivo fibroin self-assembly and secretion in the silkworm, Bombyx mori. *Int. J. Biol. Macromol.* **2021**, *169*, 473–479. [CrossRef] [PubMed]
66. Fedič, R.; Žurovec, M.; Sehnal, F. Correlation between Fibroin Amino Acid Sequence and Physical Silk Properties. *J. Biol. Chem.* **2003**, *278*, 35255–35264. [CrossRef] [PubMed]
67. Kundu, B.; Rajkhowa, R.; Kundu, S.C.; Wang, X. Silk fibroin biomaterials for tissue regenerations. *Adv. Drug Deliv. Rev.* **2013**, *65*, 457–470. [CrossRef] [PubMed]
68. Tanaka, K.; Kajiyama, N.; Ishikura, K.; Waga, S.; Kikuchi, A.; Ohtomo, K.; Takagi, T.; Mizuno, S. Determination of the site of disulfide linkage between heavy and light chains of silk fibroin produced by Bombix mori. *Biochim. Biophys. Acta Protein Struct. Mol. Enzymol.* **1999**, *1432*, 92–103. [CrossRef]
69. Mori, K.; Tanaka, K.; Kikuchi, Y.; Waga, M.; Waga, S.; Mizuno, S. Production of a chimeric fibroin light-chain polypeptide in a fibroin secretion-deficient naked pupa mutant of the silkworm Bombyx mori. *J. Mol. Biol.* **1995**, *251*, 217–228. [CrossRef] [PubMed]
70. Takei, F.; Kikuchi, Y.; Kikuchi, A.; Mizuno, S.; Shimura, K. Further evidence for importance of the subunit combination of silk fibroin in its efficient secretion from the posterior silk gland cells. *J. Cell Biol.* **1987**, *105*, 175–180. [CrossRef]
71. Sun, W.; Gregory, D.A.; Tomeh, M.A.; Zhao, X. Silk Fibroin as a Functional Biomaterial for Tissue Engineering. *Int. J. Mol. Sci.* **2021**, *22*, 1499. [CrossRef]
72. Qi, Y.; Wang, H.; Wei, K.; Yang, Y.; Zheng, R.-Y.; Kim, I.S.; Zhang, K.-Q. A Review of Structure Construction of Silk Fibroin Biomaterials from Single Structures to Multi-Level Structures. *Int. J. Mol. Sci.* **2017**, *18*, 237. [CrossRef] [PubMed]
73. Yang, C.; Yao, L.; Zhang, L. Silk sericin-based biomaterials shine in food and pharmaceutical industries. *Smart Mater. Med.* **2023**, *4*, 447–459. [CrossRef]
74. Rong, H.H.; Zhang, M.C.; Liang, X.; Liu, C.; Saadi, M.; Chen, X.Y.; Yao, L.; Zhang, Y.R.; He, N.; Hu, E.R.; et al. Demonstration of electronic synapses using a sericin-based bio-memristor. *Appl. Phys. Express* **2023**, *16*, 031007. [CrossRef]
75. Lee, K.H. Silk sericin retards the crystallization of silk fibroin. *Macromol. Rapid Commun.* **2004**, *25*, 1792–1796. [CrossRef]
76. Kundu, S.C.; Dash, B.C.; Dash, R.; Kaplan, D.L. Natural protective glue protein, sericin bioengineered by silkworms: Potential for biomedical and biotechnological applications. *Prog. Polym. Sci.* **2008**, *33*, 998–1012. [CrossRef]
77. Zhang, Y.-Q. Applications of natural silk protein sericin in biomaterials. *Biotechnol. Adv.* **2002**, *20*, 91–100. [CrossRef] [PubMed]
78. Suryawanshi, R.; Kanoujia, J.; Parashar, P.; Saraf, S.A. Sericin: A Versatile Protein Biopolymer with Therapeutic Significance. *Curr. Pharm. Des.* **2020**, *26*, 5414–5429. [CrossRef]
79. Zhou, K.; Peters, R.J. Investigating the conservation pattern of a putative second terpene synthase divalent metal binding motif in plants. *Phytochemistry* **2009**, *70*, 366–369. [CrossRef]
80. Paul, J.J.; Kircus, S.R.; Sorrell, T.N.; Ropp, P.A.; Thorp, H.H. Effects of coordinating metal ions on the mediated inhibition of trypsin by bis(benzimidazoles) and related compounds. *Inorg. Chem.* **2006**, *45*, 5126–5135. [CrossRef]
81. Qiao, X.Y.; Miller, R.; Schneck, E.; Sun, K. Influence of pH on the surface and foaming properties of aqueous silk fibroin solutions. *Soft Matter* **2020**, *16*, 3695–3704. [CrossRef]
82. Wang, Z.; Zhang, Y.; Zhang, J.; Huang, L.; Liu, J.; Li, Y.; Zhang, G.; Kundu, S.C.; Wang, L. Exploring natural silk protein sericin for regenerative medicine: An injectable, photoluminescent, cell-adhesive 3D hydrogel. *Sci. Rep.* **2014**, *4*, 7064. [CrossRef] [PubMed]
83. Khosa, M.A.; Shah, S.S.; Feng, X.S. Metal sericin complexation and ultrafiltration of heavy metals from aqueous solution. *Chem. Eng. J.* **2014**, *244*, 446–456. [CrossRef]

84. Zhong, L.-S.; Hu, J.-S.; Liang, H.-P.; Cao, A.-M.; Song, W.-G.; Wan, L.-J. Self-Assembled 3D Flowerlike Iron Oxide Nanostructures and Their Application in Water Treatment. *Adv. Mater.* **2006**, *18*, 2426–2431. [CrossRef]
85. Cao, C.-Y.; Qu, J.; Yan, W.-S.; Zhu, J.-F.; Wu, Z.-Y.; Song, W.-G. Low-Cost Synthesis of Flowerlike α-Fe2O3 Nanostructures for Heavy Metal Ion Removal: Adsorption Property and Mechanism. *Langmuir* **2012**, *28*, 4573–4579. [CrossRef] [PubMed]
86. Liu, H.; Sun, Z.; Guo, C. Chemical Modification of Silk Proteins: Current Status and Future Prospects. *Adv. Fiber Mater.* **2022**, *4*, 705–719. [CrossRef]
87. Zheng, H.; Zuo, B. Functional silk fibroin hydrogels: Preparation, properties and applications. *J. Mater. Chem. B* **2021**, *9*, 1238–1258. [CrossRef] [PubMed]
88. Bartlett, G.J.; Woolfson, D.N. On the satisfaction of backbone-carbonyl lone pairs of electrons in protein structures. *Protein Sci.* **2016**, *25*, 887–897. [CrossRef]
89. He, H.; Zhang, Y.; Wang, P.; Hu, D. Preparation of sponge-cake-like N-doped porous carbon materials derived from silk fibroin by chemical activation. *Microporous Mesoporous Mater.* **2021**, *317*, 110998. [CrossRef]
90. Li, Y.; Yao, L.; Zhang, L.; Zhang, Y.; Zheng, T.; Liu, L.; Zhang, L. Enhanced physicochemical stabilities of cyanidin-3-O-glucoside via combination with silk fibroin. *Food Chem.* **2021**, *355*, 129479. [CrossRef]
91. Yao, L.; Xu, J.; Zhang, L.; Liu, L.; Zhang, L. Nanoencapsulation of Anthocyanin by an Amphiphilic Peptide for Stability Enhancement. *Food Hydrocoll.* **2021**, *118*, 106741. [CrossRef]
92. Yao, L.; Xu, J.; Zhang, L.; Zheng, T.; Zhang, L. Physicochemical Stability-Increasing Effects of Anthocyanin via a Co-Assembly Approach with an Amphiphilic Peptide. *Food Chem.* **2021**, *362*, 130101. [CrossRef] [PubMed]
93. Kwak, H.W.; Kim, Y.; Yun, N.K.; Lee, K.H. Silk sericin microparticles as a biosorbent for hexavalent chromium ion. *Macromol. Res.* **2014**, *22*, 788–795. [CrossRef]
94. Elzoghby, A.O.; Elgohary, M.M.; Kamel, N.M. Chapter Six—Implications of Protein- and Peptide-Based Nanoparticles as Potential Vehicles for Anticancer Drugs. In *Advances in Protein Chemistry and Structural Biology*; Donev, R., Ed.; Academic Press: Cambridge, MA, USA, 2015; Volume 98, pp. 169–221.
95. Barrera-Diaz, C.E.; Lugo-Lugo, V.; Bilyeu, B. A review of chemical, electrochemical and biological methods for aqueous Cr(VI) reduction. *J. Hazard. Mater.* **2012**, *223*, 1–12. [CrossRef] [PubMed]
96. Yao, L.; Hao, M.; Zhao, F.; Wang, Y.; Zhou, Y.; Liu, Z.; An, X.; Gao, Z.; Wang, J.; Zheng, T.; et al. Fabrication of silk sericin-anthocyanin nanocoating for chelating and saturation-visualization detection of metal ions. *Nanoscale* **2022**, *14*, 17277–17289. [CrossRef] [PubMed]
97. Kwak, H.W.; Shin, M.; Yun, H.; Lee, K.H. Preparation of Silk Sericin/Lignin Blend Beads for the Removal of Hexavalent Chromium Ions. *Int. J. Mol. Sci.* **2016**, *17*, 1466. [CrossRef] [PubMed]
98. Azizian, S. Kinetic models of sorption: A theoretical analysis. *J. Colloid Interface Sci.* **2004**, *276*, 47–52. [CrossRef] [PubMed]
99. Zhang, K. *The Extraction of Silk Fibroin & Preparation, Modification and Application of Silk Fibroin Membrane*; Dong Hua University: Shanghai, China, 2015.
100. Bailey, S.E.; Olin, T.J.; Bricka, R.M.; Adrian, D.D. A review of potentially low-cost sorbents for heavy metals. *Water Res.* **1999**, *33*, 2469–2479. [CrossRef]
101. Mehta, S.K.; Gaur, J.P. Use of Algae for Removing Heavy Metal Ions From Wastewater: Progress and Prospects. *Crit. Rev. Biotechnol.* **2005**, *25*, 113–152. [CrossRef]
102. Dudev, T.; Lim, C. Competition among Metal Ions for Protein Binding Sites: Determinants of Metal Ion Selectivity in Proteins. *Chem. Rev.* **2014**, *114*, 538–556. [CrossRef]
103. Khosa, M.A.; Wu, J.; Ullah, A. Chemical modification, characterization, and application of chicken feathers as novel biosorbents. *RSC Adv.* **2013**, *3*, 20800–20810. [CrossRef]
104. Tai, H.-C.; Lim, C. Computational Studies of the Coordination Stereochemistry, Bonding, and Metal Selectivity of Mercury. *J. Phys. Chem. A* **2006**, *110*, 452–462. [CrossRef] [PubMed]
105. Koley, P.; Sakurai, M.; Aono, M. Controlled Fabrication of Silk Protein Sericin Mediated Hierarchical Hybrid Flowers and Their Excellent Adsorption Capability of Heavy Metal Ions of Pb(II), Cd(II) and Hg(II). *ACS Appl. Mater. Interfaces* **2016**, *8*, 2380–2392. [CrossRef] [PubMed]
106. Jiao, Z.Y.; Song, Y.; Jin, Y.; Zhang, C.; Peng, D.; Chen, Z.Z.; Chang, P.P.; Kundu, S.C.; Wang, G.B.; Wang, Z.; et al. In Vivo Characterizations of the Immune Properties of Sericin: An Ancient Material with Emerging Value in Biomedical Applications. *Macromol. Biosci.* **2017**, *17*, 1700229. [CrossRef] [PubMed]
107. Kundu, B.; Kurland, N.E.; Bano, S.; Patra, C.; Engel, F.B.; Yadavalli, V.K.; Kundu, S.C. Silk proteins for biomedical applications: Bioengineering perspectives. *Prog. Polym. Sci.* **2014**, *39*, 251–267. [CrossRef]
108. Gholipourmalekabadi, M.; Sapru, S.; Samadikuchaksaraei, A.; Reis, R.L.; Kaplan, D.L.; Kundu, S.C. Silk fibroin for skin injury repair: Where do things stand? *Adv. Drug Deliv. Rev.* **2020**, *153*, 28–53. [CrossRef] [PubMed]
109. Kim, D.K.; Kim, J.I.; Sim, B.R.; Khang, G. Bioengineered porous composite curcumin/silk scaffolds for cartilage regeneration. *Mater. Sci. Eng. C Mater. Biol. Appl.* **2017**, *78*, 571–578. [CrossRef] [PubMed]
110. Wang, D.; Wang, L.; Lou, Z.; Zheng, Y.; Wang, K.; Zhao, L.; Han, W.; Jiang, K.; Shen, G. Biomimetic, biocompatible and robust silk Fibroin-MXene film with stable 3D cross-link structure for flexible pressure sensors. *Nano Energy* **2020**, *78*, 105252. [CrossRef]

111. Eivazzadeh-Keihan, R.; Ganjali, F.; Aliabadi, H.A.M.; Maleki, A.; Pouri, S.; Mahdavi, M.; Shalan, A.E.; Lanceros-Méndez, S. Synthesis and characterization of cellulose, β-cyclodextrin, silk fibroin-based hydrogel containing copper-doped cobalt ferrite nanospheres and exploration of its biocompatibility. *J. Nanostruct. Chem.* **2023**, *13*, 103–113. [CrossRef]
112. Kwon, S.Y.; Chung, J.W.; Park, H.J.; Jiang, Y.Y.; Park, J.K.; Seo, Y.K. Silk and collagen scaffolds for tendon reconstruction. *Proc. Inst. Mech. Eng. Part H J. Eng. Med.* **2014**, *228*, 388–396. [CrossRef]
113. Dewair, M.; Baur, X.; Ziegler, K. Use of immunoblot technique for detection of human IgE and IgG antibodies to individual silk proteins. *J. Allergy Clin. Immunol.* **1985**, *76*, 537–542. [CrossRef]
114. Panilaitis, B.; Altman, G.H.; Chen, J.; Jin, H.-J.; Karageorgiou, V.; Kaplan, D.L. Macrophage responses to silk. *Biomaterials* **2003**, *24*, 3079–3085. [CrossRef]
115. Boonrungsiman, S.; Thongtham, N.; Suwantong, O.; Wutikhun, T.; Soykeabkaew, N.; Nimmannit, U. An improvement of silk-based scaffold properties using collagen type I for skin tissue engineering applications. *Polym. Bull.* **2018**, *75*, 685–700. [CrossRef]
116. Fu, Z.X.; Li, W.H.; Wei, J.J.; Yao, K.; Wang, Y.Q.; Yang, P.X.; Li, G.C.; Yang, Y.M.; Zhang, L.Z. Construction and Biocompatibility Evaluation of Fibroin/Sericin-Based Scaffolds. *ACS Biomater. Sci. Eng.* **2022**, *8*, 1494–1505. [CrossRef] [PubMed]
117. Aramwit, P.; Palapinyo, S.; Srichana, T.; Chottanapund, S.; Muangman, P. Silk sericin ameliorates wound healing and its clinical efficacy in burn wounds. *Arch. Dermatol. Res.* **2013**, *305*, 585–594. [CrossRef] [PubMed]
118. Wang, C.R.; Lu, Q.Y.; Xiang, Y.J.; Yin, Y.L.; Li, J.Y.; Liu, Y.L.; Wu, X.C. Enhanced biocompatibility of silk sericin/caffeic acid nanoparticles by red blood cell membranes cloaking. *Int. J. Biol. Macromol.* **2023**, *238*, 124133. [CrossRef] [PubMed]
119. Liu, B.; Song, Y.-W.; Jin, L.; Wang, Z.-J.; Pu, D.-Y.; Lin, S.-Q.; Zhou, C.; You, H.-J.; Ma, Y.; Li, J.-M.; et al. Silk structure and degradation. *Colloids Surf. B Biointerfaces* **2015**, *131*, 122–128. [CrossRef]
120. Wang, Y.Q.; Yao, D.Y.; Li, L.H.; Qian, Z.Y.; He, W.; Ding, R.; Liu, H.F.; Fan, Y.B. Effect of Electrospun Silk Fibroin-Silk Sericin Films on Macrophage Polarization and Vascularization. *ACS Biomater. Sci. Eng.* **2020**, *6*, 3502–3512. [CrossRef] [PubMed]
121. Cherng, J.H.; Chang, S.J.; Chiu, Y.K.; Chiu, Y.H.; Fang, T.J.; Chen, H.C. Low Molecular Weight Sericin Enhances the In Vitro of Immunological Modulation and Cell Migration. *Front. Bioeng. Biotechnol.* **2022**, *10*, 925197. [CrossRef]
122. Jameson, J.F.; Pacheco, M.O.; Butler, J.E.; Stoppel, W.L. Estimating Kinetic Rate Parameters for Enzymatic Degradation of Lyophilized Silk Fibroin Sponges. *Front. Bioeng. Biotechnol.* **2021**, *9*, 664306. [CrossRef]
123. Uddin, M.G.; Allardyce, B.J.; Rashida, N.; Rajkhowa, R. Mechanical, structural and biodegradation characteristics of fibrillated silk fibres and papers. *Int. J. Biol. Macromol.* **2021**, *179*, 20–32. [CrossRef]
124. Rajkhowa, R.; Hu, X.; Tsuzuki, T.; Kaplan, D.L.; Wang, X. Structure and Biodegradation Mechanism of Milled Bombyx mori Silk Particles. *Biomacromolecules* **2012**, *13*, 2503–2512. [CrossRef] [PubMed]
125. Cao, F.; Zeng, B.; Zhu, Y.; Yu, F.; Wang, M.; Song, X.; Cheng, X.; Chen, L.; Wang, X. Porous ZnO modified silk sutures with dual light defined antibacterial, healing promotion and controlled self-degradation capabilities. *Biomater. Sci.* **2020**, *8*, 250–255. [CrossRef]
126. Wang, H.-Y.; Zhang, Y.-Q.; Wei, Z.-G. Characterization of undegraded and degraded silk fibroin and its significant impact on the properties of the resulting silk biomaterials. *Int. J. Biol. Macromol.* **2021**, *176*, 578–588. [CrossRef] [PubMed]
127. Sun, M.; Li, Q.; Yu, H.; Cheng, J.; Wu, N.; Shi, W.; Zhao, F.; Shao, Z.; Meng, Q.; Chen, H.; et al. Cryo-self-assembled silk fibroin sponge as a biodegradable platform for enzyme-responsive delivery of exosomes. *Bioact. Mater.* **2022**, *8*, 505–514. [CrossRef] [PubMed]
128. Gholipourmalekabadi, M.; Mozafari, M.; Gholipourmalekabadi, M.; Nazm Bojnordi, M.; Hashemi-soteh, M.B.; Salimi, M.; Rezaei, N.; Sameni, M.; Samadikuchaksaraei, A.; Ghasemi Hamidabadi, H. In vitro and in vivo evaluations of three-dimensional hydroxyapatite/silk fibroin nanocomposite scaffolds. *Biotechnol. Appl. Biochem.* **2015**, *62*, 441–450. [CrossRef]
129. Umuhoza, D.; Yang, F.; Long, D.; Hao, Z.; Dai, J.; Zhao, A. Strategies for Tuning the Biodegradation of Silk Fibroin-Based Materials for Tissue Engineering Applications. *ACS Biomater. Sci. Eng.* **2020**, *6*, 1290–1310. [CrossRef] [PubMed]
130. Feng, Y.F.; Li, X.F.; Zhang, Q.; Ye, D.Z.; Li, M.Z.; You, R.C.; Xu, W.L. Fabrication of porous silk fibroin/cellulose nanofibril sponges with hierarchical structure using a lithium bromide solvent system. *Cellulose* **2019**, *26*, 1013–1023. [CrossRef]
131. Li, X.; Li, N.; Fan, Q.; Yan, K.; Zhang, Q.; Wang, D.; You, R. Silk fibroin scaffolds with stable silk I crystal and tunable properties. *Int. J. Biol. Macromol.* **2023**, *248*, 125910. [CrossRef]
132. Guan, Y.; You, H.; Cai, J.; Zhang, Q.; Yan, S.; You, R. Physically crosslinked silk fibroin/hyaluronic acid scaffolds. *Carbohydr. Polym.* **2020**, *239*, 116232. [CrossRef]
133. Kambe, Y.; Mizoguchi, Y.; Kuwahara, K.; Nakaoki, T.; Hirano, Y.; Yamaoka, T. Beta-sheet content significantly correlates with the biodegradation time of silk fibroin hydrogels showing a wide range of compressive modulus. *Polym. Degrad. Stab.* **2020**, *179*, 109240. [CrossRef]
134. Guo, C.; Li, C.; Kaplan, D.L. Enzymatic Degradation of Bombyx mori Silk Materials: A Review. *Biomacromolecules* **2020**, *21*, 1678–1686. [CrossRef] [PubMed]
135. Wongpinyochit, T.; Johnston, B.F.; Seib, F.P. Degradation Behavior of Silk Nanoparticles—Enzyme Responsiveness. *ACS Biomater. Sci. Eng.* **2018**, *4*, 942–951. [CrossRef] [PubMed]
136. Vepari, C.; Kaplan, D.L. Silk as a biomaterial. *Prog. Polym. Sci.* **2007**, *32*, 991–1007. [CrossRef] [PubMed]
137. Chen, S.; Liu, M.; Huang, H.; Cheng, L.; Zhao, H.-P. Mechanical properties of Bombyx mori silkworm silk fibre and its corresponding silk fibroin filament: A comparative study. *Mater. Des.* **2019**, *181*, 108077. [CrossRef]
138. Lujerdean, C.; Baci, G.M.; Cucu, A.A.; Dezmirean, D.S. The Contribution of Silk Fibroin in Biomedical Engineering. *Insects* **2022**, *13*, 286. [CrossRef] [PubMed]

139. Altman, G.H.; Diaz, F.; Jakuba, C.; Calabro, T.; Horan, R.L.; Chen, J.; Lu, H.; Richmond, J.; Kaplan, D.L. Silk-based biomaterials. *Biomaterials* **2003**, *24*, 401–416. [CrossRef] [PubMed]
140. Guo, C.C.; Li, C.M.; Mu, X.; Kaplan, D.L. Engineering silk materials: From natural spinning to artificial processing. *Appl. Phys. Rev.* **2020**, *7*, 011313. [CrossRef]
141. Johari, N.; Moroni, L.; Samadikuchaksaraei, A. Tuning the conformation and mechanical properties of silk fibroin hydrogels. *Eur. Polym. J.* **2020**, *134*, 109842. [CrossRef]
142. Vidya, M.; Rajagopal, S. Silk fibroin: A promising tool for wound healing and skin regeneration. *Int. J. Polym. Sci.* **2021**, *2021*, 9069924. [CrossRef]
143. Park, C.J.; Ryoo, J.; Ki, C.S.; Kim, J.W.; Kim, I.S.; Bae, D.G.; Um, I.C. Effect of molecular weight on the structure and mechanical properties of silk sericin gel, film, and sponge. *Int. J. Biol. Macromol.* **2018**, *119*, 821–832. [CrossRef]
144. Zhu, Z.; Ling, S.; Yeo, J.; Zhao, S.; Tozzi, L.; Buehler, M.J.; Omenetto, F.; Li, C.; Kaplan, D.L. High-Strength, Durable All-Silk Fibroin Hydrogels with Versatile Processability toward Multifunctional Applications. *Adv. Funct. Mater.* **2018**, *28*, 1704757. [CrossRef] [PubMed]
145. Li, J.; Illeperuma, W.R.K.; Suo, Z.; Vlassak, J.J. Hybrid Hydrogels with Extremely High Stiffness and Toughness. *ACS Macro Lett.* **2014**, *3*, 520–523. [CrossRef] [PubMed]
146. Nakayama, D.; Wu, F.; Mohanty, A.K.; Hirai, S.; Misra, M. Biodegradable Composites Developed from PBAT/PLA Binary Blends and Silk Powder: Compatibilization and Performance Evaluation. *ACS Omega* **2018**, *3*, 12412–12421. [CrossRef] [PubMed]
147. Sahoo, J.K.; Hasturk, O.; Falcucci, T.; Kaplan, D.L. Silk chemistry and biomedical material designs. *Nat. Rev. Chem.* **2023**, *7*, 302–318. [CrossRef] [PubMed]
148. Falcucci, T.; Presley, K.F.; Choi, J.; Fizpatrick, V.; Barry, J.; Kishore Sahoo, J.; Ly, J.T.; Grusenmeyer, T.A.; Dalton, M.J.; Kaplan, D.L. Degradable Silk-Based Subcutaneous Oxygen Sensors. *Adv. Funct. Mater.* **2022**, *32*, 2202020. [CrossRef]
149. Gonzalez-Obeso, C.; Hartzell, E.J.; Scheel, R.A.; Kaplan, D.L. Delivering on the promise of recombinant silk-inspired proteins for drug delivery. *Adv. Drug Deliv. Rev.* **2023**, *192*, 114622. [CrossRef] [PubMed]
150. Hu, X.; Shmelev, K.; Sun, L.; Gil, E.-S.; Park, S.-H.; Cebe, P.; Kaplan, D.L. Regulation of Silk Material Structure by Temperature-Controlled Water Vapor Annealing. *Biomacromolecules* **2011**, *12*, 1686–1696. [CrossRef]
151. Wu, J.; Wang, J.; Zhang, J.; Zheng, Z.; Kaplan, D.L.; Li, G.; Wang, X. Oral Delivery of Curcumin Using Silk Nano- and Microparticles. *ACS Biomater. Sci. Eng.* **2018**, *4*, 3885–3894. [CrossRef]
152. Reizabal, A.; Costa, C.M.; Pérez-Álvarez, L.; Vilas-Vilela, J.L.; Lanceros-Méndez, S. The New Silk Road: Silk Fibroin Blends and Composites for Next Generation Functional and Multifunctional Materials Design. *Polym. Rev.* **2023**, *63*, 1014–1077. [CrossRef]
153. Holland, C.; Numata, K.; Rnjak-Kovacina, J.; Seib, F.P. The Biomedical Use of Silk: Past, Present, Future. *Adv. Healthc. Mater.* **2019**, *8*, 1800465. [CrossRef]
154. Agudelo, W.; Montoya, Y.; Garcia-Garcia, A.; Restrepo-Osorio, A.; Bustamante, J. Electrochemical and Electroconductive Behavior of Silk Fibroin Electrospun Membrane Coated with Gold or Silver Nanoparticles. *Membranes* **2022**, *12*, 1154. [CrossRef] [PubMed]
155. Liu, Q.; Wang, X.; Zhou, Y.; Tan, X.; Xie, X.; Li, Y.; Dong, H.; Tang, Z.; Zhao, P.; Xia, Q. Dynamic Changes and Characterization of the Metal Ions in the Silk Glands and Silk Fibers of Silkworm. *Int. J. Mol. Sci.* **2023**, *24*, 6556. [CrossRef]
156. Gao, Z.F.; Zheng, L.L.; Fu, W.L.; Zhang, L.; Li, J.Z.; Chen, P. Feeding Alginate-Coated Liquid Metal Nanodroplets to Silkworms for Highly Stretchable Silk Fibers. *Nanomaterials* **2022**, *12*, 1177. [CrossRef] [PubMed]
157. Shao, P.; Qiu, Q.; Xiao, J.; Zhu, Y.; Sun, P. Chemical Stability and in vitro release properties of β-carotene in emulsions stabilized by Ulva fasciata polysaccharide. *Int. J. Biol. Macromol.* **2017**, *102*, 225–231. [CrossRef] [PubMed]
158. Du, Z.; Xu, N.; Yang, Y.; Li, G.; Tai, Z.; Li, N.; Sun, Y. Study on internal structure of casein micelles in reconstituted skim milk powder. *Int. J. Biol. Macromol.* **2023**, *224*, 437–452. [CrossRef]
159. He, J.X.; Jia, G.X.; Cui, S.Z.; Wang, S.Y.; Gao, Y.Y. Chemical Modification of Bombyx mori Silk with Calcium-Salt Treatment and Subsequent Glycerin Triglycidyl Ether Crosslinking. *J. Appl. Polym. Sci.* **2010**, *118*, 3260–3268. [CrossRef]
160. Drnovsek, N.; Kocen, R.; Gantar, A.; Drobnic-Kosorok, M.; Leonardi, A.; Krizaj, I.; Recnik, A.; Novak, S. Size of silk fibroin beta-sheet domains affected by Ca^{2+}. *J. Mater. Chem. B* **2016**, *4*, 6597–6608. [CrossRef] [PubMed]
161. Zhou, Q.; Chen, G.; Tang, X. Optimal Technology of Silk Weighted by Dying With Dioscorea Cirrhosa Extract and Effect of Post-treatment With Metal Ions on its Performance. *Acta Sericol. Sin.* **2008**, *34*, 694–700. [CrossRef]
162. Hua, J.S.; You, H.N.; Li, X.F.; You, R.C.; Ma, L.K. Cu(II) ion loading in silk fibroin scaffolds with silk I structure. *Int. J. Biol. Macromol.* **2020**, *158*, 275–281. [CrossRef]
163. Zhao, Y.Y.; Zhou, L.X. Theoretical study on the interaction between metal cations and dimethyl phosphate anion. *Chin. J. Struct. Chem.* **2004**, *23*, 540–546. [CrossRef]
164. Zhang, W.; Wang, M.; Guan, J.-P.; Tang, R.-C.; Qiao, Y.-F. Casein phosphopeptide-metal salts combination: A novel route for imparting the durable flame retardancy to silk. *J. Taiwan Inst. Chem. Eng.* **2019**, *101*, 1–7. [CrossRef]
165. Boyle, A.L.; Rabe, M.; Crone, N.S.A.; Rhys, G.G.; Soler, N.; Voskamp, P.; Pannu, N.S.; Kros, A. Selective coordination of three transition metal ions within a coiled-coil peptide scaffold. *Chem. Sci.* **2019**, *10*, 7456–7465. [CrossRef] [PubMed]
166. Zong, X.-H.; Zhou, P.; Shao, Z.-Z.; Chen, S.-M.; Chen, X.; Hu, B.-W.; Deng, F.; Yao, W.-H. Effect of pH and Copper(II) on the Conformation Transitions of Silk Fibroin Based on EPR, NMR, and Raman Spectroscopy. *Biochemistry* **2004**, *43*, 11932–11941. [CrossRef] [PubMed]

167. Wang, X.; Li, Y.; Liu, Q.S.; Chen, Q.M.; Xia, Q.Y.; Zhao, P. In vivo effects of metal ions on conformation and mechanical performance of silkworm silks. *Biochim. Biophys. Acta Gen. Subj.* **2017**, *1861*, 567–576. [CrossRef] [PubMed]
168. Leal, S.S.; Botelho, H.M.; Gomes, C.M. Metal ions as modulators of protein conformation and misfolding in neurodegeneration. *Coord. Chem. Rev.* **2012**, *256*, 2253–2270. [CrossRef]
169. Yan, B.; Zhou, Q.; Xing, T.; Chen, G. Dopamine-Dyed and Functionally Finished Silk with Rapid Oxidation Polymerization. *Polymers* **2018**, *10*, 728. [CrossRef] [PubMed]
170. Yan, B.; Zhou, Q.; Zhu, X.; Guo, J.; Mia, S.; Yan, X.; Chen, G.; Xing, T. A superhydrophobic bionic coating on silk fabric with flame retardancy and UV shielding ability. *Appl. Surf. Sci.* **2019**, *483*, 929–939. [CrossRef]
171. Yan, J.; Xia, D.; Zhou, W.; Li, Y.; Xiong, P.; Li, Q.; Wang, P.; Li, M.; Zheng, Y.; Cheng, Y. pH-responsive silk fibroin-based CuO/Ag micro/nano coating endows polyetheretherketone with synergistic antibacterial ability, osteogenesis, and angiogenesis. *Acta Biomater.* **2020**, *115*, 220–234. [CrossRef]
172. Zheng, H.; Huang, Z.; Chen, T.; Sun, Y.; Chen, S.; Bu, G.; Guan, H. Gallium ions incorporated silk fibroin hydrogel with antibacterial efficacy for promoting healing of Pseudomonas aeruginosa-infected wound. *Front. Chem.* **2022**, *10*, 1017548. [CrossRef]
173. Velmurugan, P.; Shim, J.; Bang, K.-S.; Oh, B.-T. Gold nanoparticles mediated coloring of fabrics and leather for antibacterial activity. *J. Photochem. Photobiol. B Biol.* **2016**, *160*, 102–109. [CrossRef]
174. Kiro, A.; Bajpai, J.; Bajpai, A.K. Designing of silk and ZnO based antibacterial and noncytotoxic bionanocomposite films and study of their mechanical and UV absorption behavior. *J. Mech. Behav. Biomed. Mater.* **2017**, *65*, 281–294. [CrossRef]
175. Yang, C.M.; Lee, J.; Lee, H.; Park, W.H. ZnO nanoparticle-embedded modified silk fibroin-tannin multifunctional hydrogel. *Int. J. Biol. Macromol.* **2022**, *210*, 1–10. [CrossRef] [PubMed]
176. Prakash, N.; Vendan, S.A.; Sudha, P.N.; Renganathan, N.G. Biodegradable Polymer-Based Ternary Blends for Adsorption of Heavy Metal From Simulated Industrial Wastewater. *Synth. React. Inorg. Met. Org. Nano Met. Chem.* **2016**, *46*, 1664–1674. [CrossRef]
177. Ki, C.S.; Gang, E.H.; Um, I.C.; Park, Y.H. Nanofibrous membrane of wool keratose/silk fibroin blend for heavy metal ion adsorption. *J. Membr. Sci.* **2007**, *302*, 20–26. [CrossRef]
178. Baek, D.H.; Ki, C.S.; Um, I.C.; Park, Y.H. Metal ion adsorbability of electrospun wool keratose/silk fibroin blend nanofiber mats. *Fibers Polym.* **2007**, *8*, 271–277. [CrossRef]
179. Ishikawa, S.-I.; Suyama, K.; Arihara, K.; Itoh, M. Selective recovery of uranium and thorium ions from dilute aqueous solutions by animal biopolymers. *Biol. Trace Elem. Res.* **2002**, *86*, 227–236. [CrossRef] [PubMed]
180. Aslani, M.A.A.; Eral, M.; Akyil, S. Separation of thorium from aqueous solution using silk fibroin. *J. Radioanal. Nucl. Chem.* **1998**, *238*, 123–127. [CrossRef]
181. Yalcin, E.; Gedikli, S.; Cabuk, A.; Karahaliloglu, Z.; Demirbilek, M.; Bayram, C.; Sam, M.; Saglam, N.; Denkbas, E.B. Silk fibroin/nylon-6 blend nanofilter matrix for copper removal from aqueous solution. *Clean Technol. Environ. Policy* **2015**, *17*, 921–934. [CrossRef]
182. Denish, P.R.; Fenger, J.-A.; Powers, R.; Sigurdson, G.T.; Grisanti, L.; Guggenheim, K.G.; Laporte, S.; Li, J.; Kondo, T.; Magistrato, A.; et al. Discovery of a natural cyan blue: A unique food-sourced anthocyanin could replace synthetic brilliant blue. *Sci. Adv.* **2021**, *7*, 7871. [CrossRef]
183. Pereira, C.D.; Techy, J.G.; Ganzarolli, E.M.; Quináia, S.P. Chromium fractionation and speciation in natural waters. *J. Environ. Monit.* **2012**, *14*, 1559–1564. [CrossRef]
184. Zhang, Y.; Li, M.; Niu, Q.Q.; Gao, P.F.; Zhang, G.M.; Dong, C.; Shuang, S.M. Gold nanoclusters as fluorescent sensors for selective and sensitive hydrogen sulfide detection. *Talanta* **2017**, *171*, 143–151. [CrossRef] [PubMed]
185. Chen, X.L.; Ren, X.J.; Gao, X.Y. Peptide or Protein-Protected Metal Nanoclusters for Therapeutic Application. *Chin. J. Chem.* **2022**, *40*, 267–274. [CrossRef]
186. Yu, Y.; Lee, W.D.; Tan, Y.N. Protein-protected gold/silver alloy nanoclusters in metal-enhanced singlet oxygen generation and their correlation with photoluminescence. *Mater. Sci. Eng. C Mater. Biol. Appl.* **2020**, *109*, 110525. [CrossRef] [PubMed]
187. Zhang, G.M.; Wang, R.R.; Shi, L.H.; Zhang, C.H.; Zhang, Y.; Zhou, Y.; Dong, C.; Li, G.; Shuang, S.M. Aggregation/assembly induced emission based on silk fibroin-templated fluorescent copper nanoclusters for "turn-on" detection of S^{2-}. *Sens. Actuators B Chem.* **2019**, *279*, 361–368. [CrossRef]
188. Zhang, G.M.; Xu, T.; Du, H.Z.; Qiao, Y.Y.; Guo, X.H.; Shi, L.H.; Zhang, Y.; Shuang, S.M.; Dong, C.; Ma, H.M. A reversible fluorescent pH-sensing system based on the one-pot synthesis of natural silk fibroin-capped copper nanoclusters. *J. Mater. Chem. C* **2016**, *4*, 3540–3545. [CrossRef]
189. Yang, W.; Guo, W.; Zhang, B.; Chang, J. Synthesis of Noble Metal Nanoclusters Based on Protein and Peptide as a Template. *Acta Chim. Sin.* **2014**, *72*, 1209–1217. [CrossRef]
190. Shiang, Y.-C.; Huang, C.-C.; Chen, W.-Y.; Chen, P.-C.; Chang, H.-T. Fluorescent gold and silver nanoclusters for the analysis of biopolymers and cell imaging. *J. Mater. Chem.* **2012**, *22*, 12972–12982. [CrossRef]
191. Söptei, B.; Naszályi Nagy, L.; Baranyai, P.; Szabó, I.; Mező, G.; Hudecz, F.; Bóta, A. On the selection and design of proteins and peptide derivatives for the production of photoluminescent, red-emitting gold quantum clusters. *Gold Bull.* **2013**, *46*, 195–203. [CrossRef]
192. Chen, Y.; Wang, Y.; Wang, C.; Li, W.; Zhou, H.; Jiao, H.; Lin, Q.; Yu, C. Papain-directed synthesis of luminescent gold nanoclusters and the sensitive detection of Cu^{2+}. *J. Colloid Interface Sci.* **2013**, *396*, 63–68. [CrossRef]
193. Jiang, Y.K.; Xu, M.; Yadavalli, V.K. Silk Fibroin-Sheathed Conducting Polymer Wires as Organic Connectors for Biosensors. *Biosensors* **2019**, *9*, 103. [CrossRef]

194. Cai, J.Y.; Wang, Q.S.; Li, X.F.; Guan, Y.P.; He, L.Y.; Yan, S.Q.; You, R.C.; Zhang, Q. Water-stable natural silk nanofibril composite films for electrical devices. *Mater. Today Commun.* **2020**, *22*, 100776. [CrossRef]
195. Sasso, L.; Gerrard, J.A. Chapter 1—Self-Assembled Biological Nanofibers for Biosensor Applications. In *Micro and Nanofabrication Using Self-Assembled Biological Nanostructures*; Castillo-León, J., Svendsen, W.E., Eds.; William Andrew Publishing: Oxford, UK, 2015; pp. 1–20.
196. Tao, H.; Kaplan, D.L.; Omenetto, F.G. Silk Materials–A Road to Sustainable High Technology. *Adv. Mater.* **2012**, *24*, 2824–2837. [CrossRef] [PubMed]
197. Huang, X.W.; Liang, H.; Li, Z.; Zhou, J.; Chen, X.; Bai, S.M.; Yang, H.H. Monodisperse phase transfer and surface bioengineering of metal nanoparticles via a silk fibroin protein corona. *Nanoscale* **2017**, *9*, 2695–2700. [CrossRef] [PubMed]
198. Zhang, P.; Lan, J.; Wang, Y.; Xiong, Z.H.; Huang, C.Z. Luminescent golden silk and fabric through in situ chemically coating pristine-silk with gold nanoclusters. *Biomaterials* **2015**, *36*, 26–32. [CrossRef] [PubMed]
199. Patil, A.C.; Bandla, A.; Liu, Y.-H.; Luo, B.; Thakor, N.V. Nontransient silk sandwich for soft, conformal bionic links. *Mater. Today* **2020**, *32*, 68–83. [CrossRef]
200. Lee, M.; Jeon, H.; Kim, S. A Highly Tunable and Fully Biocompatible Silk Nanoplasmonic Optical Sensor. *Nano Lett.* **2015**, *15*, 3358–3363. [CrossRef] [PubMed]
201. Benvidi, A.; Banaei, M.; Tezerjani, M.D.; Molahosseini, H.; Jahanbani, S. Impedimetric PSA aptasensor based on the use of a glassy carbon electrode modified with titanium oxide nanoparticles and silk fibroin nanofibers. *Microchim. Acta* **2017**, *185*, 50. [CrossRef] [PubMed]
202. Kwon, H.; Kim, S. Chemically Tunable, Biocompatible, and Cost-Effective Metal–Insulator–Metal Resonators Using Silk Protein and Ultrathin Silver Films. *ACS Photonics* **2015**, *2*, 1675–1680. [CrossRef]
203. Molinnus, D.; Drinic, A.; Iken, H.; Kröger, N.; Zinser, M.; Smeets, R.; Köpf, M.; Kopp, A.; Schöning, M.J. Towards a flexible electrochemical biosensor fabricated from biocompatible Bombyx mori silk. *Biosens. Bioelectron.* **2021**, *183*, 113204. [CrossRef]
204. Promphet, N.; Phamonpon, W.; Karintrithip, W.; Rattanawaleedirojn, P.; Saengkiettiyut, K.; Boonyongmaneerat, Y.; Rodthongkum, N. Carbonization of self-reduced AuNPs on silk as wearable skin patches for non-invasive sweat urea detection. *Int. J. Biol. Macromol.* **2023**, *242*, 124757. [CrossRef]
205. Sun, K.; Wang, C.; Tian, J.H.; Zhang, Z.; Zeng, N.; Yin, R.; Duan, W.X.; Hou, Q.; Zhao, Y.M.; Wu, H.K.; et al. Magnetic-Driven Broadband Epsilon-Near-Zero Materials at Radio Frequency. In *Advanced Functional Materials*; Wiley: New York, NY, USA, 2023.
206. Wu, R.; Ma, L.; Hou, C.; Meng, Z.; Guo, W.; Yu, W.; Yu, R.; Hu, F.; Liu, X.Y. Silk Composite Electronic Textile Sensor for High Space Precision 2D Combo Temperature-Pressure Sensing. *Small* **2019**, *15*, 1901558. [CrossRef] [PubMed]
207. He, Y.; Gui, Q.; Liao, S.; Jia, H.; Wang, Y. Coiled Fiber-Shaped Stretchable Thermal Sensors for Wearable Electronics. *Adv. Mater. Technol.* **2016**, *1*, 1600170. [CrossRef]
208. Harada, S.; Kanao, K.; Yamamoto, Y.; Arie, T.; Akita, S.; Takei, K. Fully Printed Flexible Fingerprint-like Three-Axis Tactile and Slip Force and Temperature Sensors for Artificial Skin. *ACS Nano* **2014**, *8*, 12851–12857. [CrossRef] [PubMed]
209. Zhao, X.-H.; Ma, S.-N.; Long, H.; Yuan, H.; Tang, C.Y.; Cheng, P.K.; Tsang, Y.H. Multifunctional Sensor Based on Porous Carbon Derived from Metal–Organic Frameworks for Real Time Health Monitoring. *ACS Appl. Mater. Interfaces* **2018**, *10*, 3986–3993. [CrossRef] [PubMed]
210. Tao, H.; Brenckle, M.A.; Yang, M.; Zhang, J.; Liu, M.; Siebert, S.M.; Averitt, R.D.; Mannoor, M.S.; McAlpine, M.C.; Rogers, J.A.; et al. Silk-Based Conformal, Adhesive, Edible Food Sensors. *Adv. Mater.* **2012**, *24*, 1067–1072. [CrossRef] [PubMed]
211. Mulyaningsih, R.D.; Pratiwi, R.; Hasanah, A.N. An Update on the Use of Natural Pigments and Pigment Nanoparticle Adducts for Metal Detection Based on Colour Response. *Biosensors* **2023**, *13*, 554. [CrossRef] [PubMed]
212. Shobana, J.; Kalaivani, D.; Porchezhiyan, V.; Noorjahan, S.E. Syzgium cumini extract- a natural naked eye colorimetric sensor for selective and sensitive detection of Fe^{2+} in aqueous medium. *Groundw. Sustain. Dev.* **2023**, *20*, 100866. [CrossRef]
213. Parizadeh, P.; Moeinpour, F.; Mohseni-Shahri, F.S. Anthocyanin-induced color changes in bacterial cellulose nanofibers for the accurate and selective detection of Cu(II) in water samples. *Chemosphere* **2023**, *326*, 138459. [CrossRef]
214. Zhang, L.; Yao, L.; Zhao, F.; Yu, A.; Zhou, Y.; Wen, Q.; Wang, J.; Zheng, T.; Chen, P. Protein and Peptide-based Nanotechnology for Enhancing Stability, Bioactivity, and Delivery of Anthocyanins. *Adv. Healthc. Mater.* **2023**, *12*, 2300473. [CrossRef]
215. Rahman, M.; Dutta, N.K.; Choudhury, N.R. Microroughness induced biomimetic coating for biodegradation control of magnesium. *Mater. Sci. Eng. C Mater. Biol. Appl.* **2021**, *121*, 111811. [CrossRef]
216. Hu, M.M.; Hu, T.; Cheng, R.F.; Yang, J.X.; Cui, C.; Zhang, C.; Wang, X.H. MXene-coated silk-derive d carbon cloth toward flexible electrode for supercapacitor application. *J. Energy Chem.* **2018**, *27*, 161–166. [CrossRef]
217. Zhou, J.; Zhang, R.; Xu, R.; Li, Y.; Tian, W.; Gao, M.; Wang, M.; Li, D.; Liang, X.; Xie, L.; et al. Super-Assembled Hierarchical Cellulose Aerogel-Gelatin Solid Electrolyte for Implantable and Biodegradable Zinc Ion Battery. *Adv. Funct. Mater.* **2022**, *32*, 2111406. [CrossRef]
218. Khairy, M.; Kamal, R.; Mousa, M.A. Preparation and physical properties of conductive silk fabrics used in wearable clothes and flexible supercapacitors. *J. Ind. Text.* **2022**, *52*, 15280837221130512. [CrossRef]
219. Cai, H.; Wang, Y.; Xu, M.; Cheng, L.; Liu, Z.; Li, Z.; Dai, F. Low cost, green and effective preparation of multifunctional flexible silk fabric electrode with ultra-high capacitance retention. *Carbon* **2022**, *188*, 197–208. [CrossRef]
220. Badawy, I.M.; Ali, B.A.; Abbas, W.A.; Allam, N.K. Natural silk for energy and sensing applications: A review. *Environ. Chem. Lett.* **2021**, *19*, 2141–2155. [CrossRef]

221. Zhang, H.; Li, Y.; Gao, G.; Song, T.Y.; Zhang, K.Y.; Yao, Y.C. Composite cathodes and modified separators based on corn-silk-based porous carbon for high performance lithium-sulfur batteries. *J. Mater. Res. Technol.* **2022**, *19*, 1590–1599. [CrossRef]
222. Zhu, M.H.; Ran, Q.; Huang, H.H.; Xie, Y.F.; Zhong, M.X.; Lu, G.Y.; Bai, F.Q.; Lang, X.Y.; Jia, X.T.; Chao, D.M. Interface Reversible Electric Field Regulated by Amphoteric Charged Protein-Based Coating Toward High-Rate and Robust Zn Anode. *Nano-Micro Lett.* **2022**, *14*, 219. [CrossRef]
223. Pan, P.; Zhang, M.; Cheng, Z.; Jiang, L.; Mao, J.; Ni, C.; Chen, Q.; Zeng, Y.; Hu, Y.; Fu, K. Garnet ceramic fabric-reinforced flexible composite solid electrolyte derived from silk template for safe and long-term stable All-Solid-State lithium metal batteries. *Energy Storage Mater.* **2022**, *47*, 279–287. [CrossRef]
224. Zhi, J.; Li, S.; Han, M.; Chen, P. Biomolecule-guided cation regulation for dendrite-free metal anodes. *Sci. Adv.* **2020**, *6*, 1342. [CrossRef]
225. Li, B.; Zhang, X.T.; Wang, T.L.; He, Z.X.; Lu, B.A.; Liang, S.Q.; Zhou, J. Interfacial Engineering Strategy for High-Performance Zn Metal Anodes. *Nano-Micro Lett.* **2022**, *14*, 6. [CrossRef]
226. Han, J.S.; Zhang, L.J.; Duan, L.Q.; Liu, L.; Xiao, X.W.; Xin, X.; Li, X. Uniform Li-deposition induced by Ni-catalyzing graphitization of natural carbon materials in lithium metal batteries. *ChemNanoMat* **2023**, *9*, e202300194. [CrossRef]
227. Li, X.; Yuan, L.; Liu, D.; Liao, M.; Chen, J.; Yuan, K.; Xiang, J.; Li, Z.; Huang, Y. Elevated Lithium Ion Regulation by a "Natural Silk" Modified Separator for High-Performance Lithium Metal Anode. *Adv. Funct. Mater.* **2021**, *31*, 2100537. [CrossRef]
228. Lu, J.; Yang, J.; Zhang, Z.; Wang, C.; Xu, J.; Wang, T. Silk Fibroin Coating Enables Dendrite-free Zinc Anode for Long-Life Aqueous Zinc-Ion Batteries. *ChemSusChem* **2022**, *15*, e202200656. [CrossRef] [PubMed]
229. Zhang, L.; Zhang, T.; Xin, W.; Peng, H.; Yan, Z.; Zhu, Z. Additive engineering for a hydrophilic/zincophilic polymeric layer towards dendrite-free zinc anode. *Mater. Today Energy* **2022**, *29*, 101130. [CrossRef]
230. Dalwadi, S.; Goel, A.; Kapetanakis, C.; Salas-de la Cruz, D.; Hu, X. The Integration of Biopolymer-Based Materials for Energy Storage Applications: A Review. *Int. J. Mol. Sci.* **2023**, *24*, 3975. [CrossRef] [PubMed]
231. Seo, Y.; Ha, H.; Cheong, J.Y.; Leem, M.; Darabi, S.; Matteini, P.; Muller, C.; Yun, T.G.; Hwang, B. Highly Reliable Yarn-Type Supercapacitor Using Conductive Silk Yarns with Multilayered Active Materials. *J. Nat. Fibers* **2022**, *19*, 835–846. [CrossRef]
232. Sun, Y.; Xue, S.; Sun, J.; Li, X.; Ou, Y.; Zhu, B.; Demir, M. Silk-derived nitrogen-doped porous carbon electrodes with enhanced ionic conductivity for high-performance supercapacitors. *J. Colloid Interface Sci.* **2023**, *645*, 297–305. [CrossRef]
233. Huang, W.; Zhang, A.; Liang, H.; Liu, R.; Cai, J.; Cui, L.; Liu, J. Novel fabrication of hollow and spinous $NiCo_2S_4$ nanotubes templated by natural silk for all-solid-state asymmetric supercapacitors. *J. Colloid Interface Sci.* **2019**, *549*, 140–149. [CrossRef]
234. Song, P.; Tao, J.; He, X.; Sun, Y.; Shen, X.; Zhai, L.; Yuan, A.; Zhang, D.; Ji, Z.; Li, B. Silk-inspired stretchable fiber-shaped supercapacitors with ultrahigh volumetric capacitance and energy density for wearable electronics. *Chem. Eng. J.* **2020**, *386*, 124024. [CrossRef]
235. Ju, Y.X.; Song, P.; Wang, P.Y.; Chen, X.X.; Chen, T.; Yao, X.H.; Zhao, W.G.; Zhang, D.Y. Cartilage structure-inspired elastic silk nanofiber network hydrogel for stretchable and high-performance supercapacitors. *Int. J. Biol. Macromol.* **2023**, *242*, 124912. [CrossRef]
236. Lu, R.Q.; Sam, D.K.; Gong, S.H.; Wang, W.B.; Ge, D.D.; Liu, J.; Zhang, Y.J.; Gao, M.; Lv, X.M. Silk fibroin derived porous carbon aerogels confined hyperdispersed Rh nanoparticles to achieve electrocatalytic hydrogen evolution under high current density. *Diam. Relat. Mater.* **2022**, *128*, 109292. [CrossRef]
237. Chen, T.; Peng, Y.; Qiu, M.; Yi, C.; Xu, Z. Protein-supported transition metal catalysts: Preparation, catalytic applications, and prospects. *Int. J. Biol. Macromol.* **2023**, *230*, 123206. [CrossRef] [PubMed]
238. Chen, J.; Liu, J.; Yang, W.; Pei, Y. Collagen and Silk Fibroin as Promising Candidates for Constructing Catalysts. *Polymers* **2023**, *15*, 375. [CrossRef] [PubMed]
239. Xu, S.J.; Yong, L.; Wu, P.Y. One-Pot, Green, Rapid Synthesis of Flowerlike Gold Nanoparticles/Reduced Graphene Oxide Composite with Regenerated Silk Fibroin As Efficient Oxygen Reduction Electrocatalysts. *ACS Appl. Mater. Interfaces* **2013**, *5*, 654–662. [CrossRef] [PubMed]
240. Liu, J.T.; Wei, L.L.; Cao, C.; Zhang, F.T.; Lang, F.Z.; Wang, H.Q.; Yang, H.J.; Shen, J.Q. Salt-induced silk gel-derived N and trace Fe co-doped 3D porous carbon as an oxygen reduction catalyst in microbial fuel cells. *Nanoscale* **2019**, *11*, 13431–13439. [CrossRef]
241. Wang, C.; Chen, W.; Xia, K.; Xie, N.; Wang, H.; Zhang, Y. Silk-Derived 2D Porous Carbon Nanosheets with Atomically-Dispersed Fe-Nx-C Sites for Highly Efficient Oxygen Reaction Catalysts. *Small* **2019**, *15*, 1804966. [CrossRef]
242. Lu, R.; Sam, D.K.; Wang, W.; Gong, S.; Liu, J.; Durairaj, A.; Li, M.; Lv, X. Boron, nitrogen co-doped biomass-derived carbon aerogel embedded nickel-cobalt-iron nanoparticles as a promising electrocatalyst for oxygen evolution reaction. *J. Colloid Interface Sci.* **2022**, *613*, 126–135. [CrossRef] [PubMed]
243. Sam, D.K.; Wang, W.; Gong, S.; Sam, E.K.; Lv, X.; Wang, J.; Liu, J. CO_2 assisted synthesis of silk fibroin driven robust N-doped carbon aerogels coupled with nickel–cobalt particles as highly active electrocatalysts for HER. *Int. J. Hydrog. Energy* **2021**, *46*, 21525–21533. [CrossRef]
244. Gong, S.H.; Xiao, X.X.; Wang, W.B.; Sam, D.K.; Lu, R.Q.; Xu, Y.G.; Liu, J.; Wu, C.D.; Lv, X.M. Silk fibroin-derived carbon aerogels embedded with copper nanoparticles for efficient electrocatalytic CO_2-to-CO conversion. *J. Colloid Interface Sci.* **2021**, *600*, 412–420. [CrossRef]